Am J Cancer Res 2026;16(6):2433-2457
www.ajcr.us /ISSN:2156-6976/ajcr0171921

Original Article

LAMP5 as a novel prognostic biomarker linked to the tumor immune microenvironment in esophageal squamous cell carcinoma

Gaoyan Wang[1*], Zhijie Li[2*], Jia Liang[3], Lei Liu[4], Yan Zhao[5], Supeng Shen[3]

[1]College of Integrative Medicine, Hebei University of Chinese Medicine, Shijiazhuang 050200, Hebei, China; [2]The Experimental Center, Hebei University of Chinese Medicine, Shijiazhuang 050200, Hebei, China; [3]Biological Tissue Specimen Bank, Hebei Cancer Institute, The Fourth Hospital of Hebei Medical University, Shijiazhuang 050011, Hebei, China; [4]Cardiovascular Medicine Department, The Fourth Hospital of Hebei Medical University, Shijiazhuang 050011, Hebei, China; [5]Radiotherapy Department, The Fourth Hospital of Hebei Medical University, Shijiazhuang 050011, Hebei, China. [*]Equal contributors.

Received February 6, 2026; Accepted May 22, 2026; Epub June 15, 2026; Published June 30, 2026

Abstract: Background: Identifying reliable prognostic biomarkers and elucidating their cellular origins in the tumor microenvironment (TME) is crucial for improving esophageal squamous cell carcinoma (ESCC) management. Methods: Differentially expressed genes were identified from GSE53624 and GSE32424 datasets. LASSO-Cox regression generated a prognostic risk signature, and a nomogram was built for overall survival prediction. CIBERSORT assessed immune infiltration. Experimental validation included qPCR, immunohistochemistry, and functional assays in cell lines and clinical specimens (n = 65). Lysosomal-associated membrane protein 5 (LAMP5)-modified ESCC cells were co-cultured with $CD8^+$ T cells to assess activation and viability. A mouse subcutaneous tumor model was used for *in vivo* validation. Results: A four-gene prognostic signature was established; LAMP5 demonstrated the strongest independent prognostic value (area under the curve = 0.773). LAMP5-associated genes were enriched in immune-related pathways. Overexpression of LAMP5 promoted malignant behavior, inhibited ESCC cell apoptosis, and suppressed $CD8^+$ T cell activation. High LAMP5 expression correlated with advanced TNM stage, poor prognosis, and lymph node metastasis. *In vivo*, LAMP5 overexpression inhibited $CD8^+$ T cell activation and promoted tumor growth. Conclusion: LAMP5 is associated with immune responses in the TME and acts as a promising novel biomarker for ESCC. Its overexpression inhibits $CD8^+$ T cell activation and drives malignant progression.

Keywords: Esophageal squamous cell carcinoma, lysosomal-associated membrane protein 5, tumor microenvironment, prognostic biomarker, immune cell infiltration

Introduction

Esophageal squamous cell carcinoma (ESCC) is among the most aggressive malignancies globally, characterized by high morbidity and lethality [1, 2]. Due to the absence of typical symptoms and the presence of distant metastases, most patients are already at an intermediate or advanced stage upon admission, for whom surgical treatment combined with adjuvant radiotherapy and chemotherapy is the main therapeutic option [3]. Despite notable progress in diagnosis and treatment methods, the 5-year survival rate of ESCC patients remains below 20% [4]. Therefore, great efforts are needed to explore prognosis-related genes and therapeutic strategies for ESCC.

In recent years, emerging evidence has validated that molecular biomarkers, including protein-coding genes, long non-coding RNAs, microRNAs, and metabolism-related gene signatures, enable effective survival prediction and risk stratification in various solid tumors such as hepatocellular carcinoma [5], gastric cancer [6], colorectal cancer [7], breast cancer [8], and bladder cancer [9]. These studies highlight the critical value of molecular profiling in refining tumor prognosis evaluation. However, compared with other malignancies, ESCC fea-

https://doi.org/10.62347/WWRY9690

tures high genetic heterogeneity and a complex tumor microenvironment (TME), and the development of specific prognostic biomarkers for ESCC remains in the exploratory phase [10, 11]. More importantly, key prognostic molecules that simultaneously regulate the malignant biological behavior of ESCC cells and modulate the TME remain unidentified.

We developed a prognostic signature derived from the risk score calculated from survival-related genes in this study. The nomogram model based on N stage, TNM stage, and risk stratification was constructed, and grainyhead-like transcription factor 3 (GRHL3), lysosomal-associated membrane protein 5 (LAMP5), urokinase-type plasminogen activator (PLAU), and RAS-related protein 25 (RAB25) were shown to predict 1-, 3-, and 5-year overall survival (OS) in ESCC. This nomogram robustly stratifies ESCC survival risk and integrates with clinical staging to refine outcome prediction. In this study, we also constructed LAMP5 overexpression/knockdown cell lines by plasmid transfection and systematically explored the regulatory role of LAMP5 on the malignant progression of ESCC and on $CD8^+$ T cell infiltration in the TME, both *in vitro* and *in vivo*. LAMP5 could be an independent prognostic factor. LAMP5 was found to be a crucial gene and a possible biomarker, showing a positive link with TNM stage and lymph node metastasis, as well as a positive correlation with poor prognosis.

Materials and methods

Data information

The gene expression profiles of GSE53624 and GSE53622, along with the corresponding clinical traits of ESCC patients, were derived from the Gene Expression Omnibus database. The two datasets were based on the GPL18109 platform and contained 119 and 60 paired ESCC and normal tissues, respectively. The RNA-seq dataset GSE32424 (GPL10999 platform) was downloaded from Expression Atlas and contained seven ESCC tissues and five normal tissues. Gene symbols were annotated using the AnnoProbe and clusterProfiler packages in R (version 4.1.1) [12]. Principal component analysis between the different groups was performed using the FactoMineR and Factoextra packages in R. To identify differentially expressed genes (DEGs) in ESCC and normal tissues, the limma and DESeq2 packages were used. The DEGs were selected based on the criteria: $|logFC| \geq 2$ and $P<0.05$. The R package ggVennDiagram was used to visualize the overlapping DEGs between the two datasets.

Functional enrichment analysis

We performed Gene Ontology (GO), Kyoto Encyclopedia of Genes and Genomes (KEGG) pathway enrichment, and Gene Set Enrichment Analysis (GSEA) analyses using the clusterProfiler package in R to elucidate the biological functions of DEGs. The hallmark gene set (h.all.v7.5.1.symbols.gmt) required for subsequent analyses was obtained from the Molecular Signatures Database.

Survival analysis

Using the survival and survminer packages, the Kaplan-Meier method and univariate/multivariate Cox proportional hazards model were applied to evaluate the association between clinical traits and patient outcomes. The predictive performance of the prognostic signature for 1-, 3-, and 5-year OS was assessed using time-dependent receiver operating characteristic (ROC) curves, implemented with the R package timeROC [13].

Clinical samples

A total of 65 pairs of ESCC and adjacent normal tissue samples were collected from The Fourth Hospital of Hebei Medical University between 2014 and 2016. None of the patients for whom survival data were available had undergone any treatment; all provided informed consent prior to surgery. The specimens were confirmed by pathologists and immediately stored at -80°C after surgical resection. All tissue specimens were approved by the Human Ethics Committee of The Fourth Hospital of Hebei Medical University (No. 2022KY257).

Quantitative real-time PCR (qRT-PCR)

RNA was extracted from the tissue samples of ESCC patients using TRIzol reagent (Invitrogen, USA), and subsequent reverse transcription into complementary DNA was conducted using the GoScript™ Reverse Transcription System (Promega, USA). qRT-PCR was performed using TB Green Premix Ex Taq II FAST qPCR (CN830S,

Table 1. Primer sequences used for qRT-PCR

Gene	Forward primer (5'→3')	Reverse primer (5'→3')
GRHL3	CTGCCTCTGAAGCGTACCTG	CTCAGTCTCCCTCCGCACAT
LAMP5	CTGCAAGTGTTCTGGGTGGA	TCATGGTGACCGTCTTCTGC
PLAU	CCCCGCTTTAAGATTATTGG	CGACCCAGGTAGACGATGTAG
RAB25	TCGCTGAAAACAATGGACTGCTCTT	ATTGGTCCGGATGCTGTTCTGTCTCT
GAPDH	GAGTCAACGGATTTGGTCGTAT	ATGGGTGGAATCATATTGGAAC

qRT-PCR: Quantitative real-time PCR; GRHL3: Grainyhead-like transcription factor 3; LAMP5: Lysosomal-associated membrane protein 5; PLAU: Urokinase-type plasminogen activator; RAB25: RAS-related protein 25; GAPDH: Glyceraldehyde-3-phosphate dehydrogenase.

Takara Bio Inc., Shiga, Japan) on an ABI Prism 7300 Real-Time PCR System (Applied Biosystems, CA, USA). The reaction was carried out in a 25 μL volume system containing: 12.5 μL 2× TB Green Premix Ex Taq II Fast qPCR, 1 μL forward primer (10 μM), 1 μL reverse primer (10 μM), 2 μL complementary DNA template, and 8.5 μL nuclease-free water.

The amplification conditions were set as follows: initial denaturation at 95°C for 30 s, followed by 40 cycles of denaturation at 95°C for 5 s and annealing/extension at 60°C for 10 s. A melting curve analysis was performed from 60°C to 95°C to verify amplification specificity. GAPDH was used as the internal reference. Levels of GRHL3, LAMP5, PLAU, and RAB25 expression were determined according to the $2^{-\Delta\Delta Ct}$ method. The primer sequences used in this study are shown in **Table 1**.

Cell culture and transfection

Human ESCC cell lines (KYSE150, KYSE170, and TE1) were obtained from the American Type Culture Collection. Mouse ESCC cell mEC25 (YS25035C) was purchased from Shanghai Yaji Biological Technology Co., Ltd. (Shanghai, China). These cells were grown in RPMI 1640 (Gibco, Thermo Fisher Scientific) supplemented with 10% fetal bovine serum (F8687, Sigma-Aldrich) at 37°C with 5% CO_2. The specifically designed si-LAMP5 and pcDNA3.1-LAMP5 plasmids and negative controls (si-NC and pcDNA3.1) were synthesized by Genepharma (Shanghai, China). These plasmids were transfected into TE1 cells using Lipofectamine™ 2000 Transfection Reagent (11668027, Thermo Fisher Scientific). After 48 hours of transfection, total RNA and protein samples were collected for subsequent assays.

Cell counting kit-8 assay

After transfection with different plasmids, TE1 cells were seeded into 96-well plates (1×10^4 cells/well) and cultured for 24, 48, or 72 h. Then, 10% cell counting kit-8 reagent (96992, Sigma-Aldrich) was added and mixed thoroughly, and the plates were incubated for 2 h in the dark. OD450 values were determined with a microplate reader (SpectraMax iD3s, Molecular Devices, Shanghai, China), and cell viability was calculated based on the results [14]. Cell viability (%) = (OD450 value of experimental group/OD450 value of negative control group) × 100%.

Clone formation assay

After different treatments, TE1 cells were gently rinsed with phosphate-buffered saline (PBS). Then, 1 mL of cell suspension (1000 cells/well) was seeded into a 6-well plate. The culture medium was refreshed every 2-3 days for a total of 14 days. When obvious colony formation was observed with the naked eye, the culture was terminated. The cells were then fixed with 4% paraformaldehyde (MedChemExpress, NJ, USA) for 30 min. After staining with 1% crystal violet (C916088, Macklin, Shanghai, China) for 10 min, the plates were gently rinsed with PBS. The plates were then air-dried, and colonies were visualized using an optical microscope (Ts2R-FL, Nikon).

Scratch-wound assay

Following transfection, cells were seeded into 6-well plates (2×10^5 cells/well). Once cell confluence reached 80%, a pipette tip was used to create a uniform scratch across the cell monolayer. After that, the plates were rinsed twice with PBS to remove detached cells and debris.

Each well was supplemented with serum-free medium, and the cells were incubated for 24 hours. The wound was imaged using a light microscope immediately (0 h) and 24 h after wounding. Cell migration distance data were acquired and analyzed using ImageJ 1.54 h software (National Institutes of Health, Bethesda, MD, USA). The wound closure rate was calculated as: (scratch width at 0 h - scratch width at 24 h)/scratch width at 0 h × 100%.

Transwell assay

Matrigel (354234, Corning, Tewksbury, MA, USA) was melted at 4°C and diluted with serum-free medium at a ratio of 8:1 (medium:Matrigel). The upper surface of the Transwell chamber membrane (8 μm pore size, Corning) was evenly coated with 100 μL of diluted Matrigel and incubated at 37°C until the Matrigel solidified. Subsequently, the chambers were placed in 24-well cell culture plates. The lower chamber was filled with 500 μL of complete culture medium. Then, 100 μL of TE1 cell suspension was added to the upper chamber, and the plates were incubated for 48 hours. Following incubation, the Transwell chambers were removed, and the upper surface of the membrane was carefully wiped with a sterile cotton swab to remove non-invading cells. The chambers were then fixed with 4% paraformaldehyde for 10 min and stained with 0.1% crystal violet for 20 min. Light microscopy was used to acquire images of five randomly chosen fields of view, and invasive cells were counted.

Isolation of $CD8^+$ T cells

A total of 10 mL of peripheral blood was collected from healthy volunteers into a heparinized tube. The anticoagulated peripheral blood was then gently mixed with an equal volume of sterile PBS. Then, 5 mL of cell separation medium (P9010, Solarbio, Beijing, China) was slowly added along the inner wall of a sterile centrifuge tube to maintain a smooth interface. Diluted peripheral blood was slowly layered along the centrifuge tube wall onto the cell separation medium, forming a clear double-layer interface. After centrifugation at low speed for 10 min, the cells in the middle white membrane layer, which are peripheral blood mononuclear cells [15]. Highly pure $CD8^+$ T cells were sorted from peripheral blood mononuclear cells using the Immunomagnetic Bead $CD8^+$ T Cell Sorting Kit (11348D, Invitrogen). In a Transwell chamber, TE1 cells transfected with different plasmids were added into the lower chamber, and $CD8^+$ T cells were added into the upper chamber. The cells were co-cultured at a ratio of 1:3 (TE1:$CD8^+$ T cells) for 48 hours [16]. Before harvest, $CD8^+$ T cells were treated with a protein transport inhibitor (Brefeldin A, HY-16592, MedChemExpress) for 4 hours to retain intracellular cytokines. After co-culture, $CD8^+$ T cells were collected, rinsed with pre-cooled PBS, and then incubated with CD8 antibody (12-0088-42, Invitrogen) for 15 min in the dark. Cells were washed three times with PBS, fixed with 4% paraformaldehyde for 15 min, and then permeabilized with Permeabilization Buffer (ICB01, MULTISCIENCES, Hangzhou, China) for 15 min. After washing once with PBS, antibodies against interferon-γ (IFN-γ, ab322926, Abcam, Cambridge, MA, USA), perforin (ab86318, Abcam), tumor necrosis factor-α (TNF-α, ab215188, Abcam), and granzyme B (ab317458, Abcam) were added. After mixing, the cells were incubated for 30 min in the dark [17]. The cells were then washed twice with PBS to remove unbound primary antibodies. Finally, the fluorescence intensity was assessed using flow cytometry (BD FACSCalibur™, BD biosciences, San Jose, CA, USA), and positive $CD8^+$ T cells were analyzed using FlowJo software (v10.8, BD Biosciences).

Carboxyfluorescein succinimidyl ester (CFSE) staining

After sorting, $CD8^+$ T cells were washed twice with pre-cooled PBS. CFSE dye (HY-D0938, MedChemExpress) was added to the cell suspension to a final concentration of 5 μM. The cells were labeled at 37°C for 10 min in the dark, and complete medium was added to terminate the staining process [18]. Cells were collected and rinsed with PBS, and fluorescence intensity was examined using a BX53 fluorescence microscope (Olympus). After 48 hours of co-culture of labeled $CD8^+$ T cells with transfected TE1 cells, CFSE fluorescence intensity was measured using flow cytometry, and cell proliferation was assessed using FlowJo software.

Apoptosis assay

TE1 cells or $CD8^+$ T cells after different treatments were collected, gently rinsed with pre-cooled PBS, and then mixed with 500 μL of

Annexin V binding buffer (E-CK-A217, Elabscience Biotechnology Co., Ltd., Wuhan, China) to adjust the cell concentration to 1×10^6 cells/mL. Then, 5 μL of Annexin-V-APC reagent and 5 μL of propidium iodide staining solution were added sequentially and mixed thoroughly at 25°C. After staining for 15 min in the dark, fluorescence was measured using flow cytometry, and the data were analyzed using FlowJo software to calculate the apoptosis rate.

Lactate dehydrogenase (LDH) assay

LDH Cytotoxicity Assay Kit (C0016, Beyotime, Shanghai, China) was used to detect $CD8^+$ T cell-mediated cytotoxicity [19]. After 48 hours of co-culture between $CD8^+$ T cells and TE1 cells, the supernatant from each group was collected by centrifugation. According to the manufacturer's instructions, the supernatant (120 μL) was thoroughly mixed with LDH detection working solution (60 μL), and the mixture was incubated in the dark for 30 min. The OD490 value of each sample was measured using a microplate reader to calculate cytotoxicity.

Mouse subcutaneous graft tumor model

Female C57BL/6 mice (5-6 weeks old, 15-17 g) were purchased from Vital River Laboratories (Beijing, China) and housed at 25±1°C, 50±10% relative humidity, under a 12-hour light/dark cycle. After one week of acclimatization, mice were randomly divided into four groups (n = 6 per group) using a random number table. Then, 5×10^5 mEC25 cells transfected with si-NC, si-LAMP5, pcDNA3.1-NC, or pcDNA3.1-LAMP5 were injected into the right axillary region of each mouse [20]. Tumor growth was observed weekly, and the long diameter (a) and short diameter (b) of the tumor were assessed using calipers. The tumor size was then calculated to establish a tumor growth curve. Tumor volume (mm^3) was calculated using the formula: Volume = $(a \times b^2)/2$, where a is the longest diameter and b is the shortest diameter. After 4 weeks, the mice were anesthetized with 2% isoflurane inhalation. Retro-orbital blood was then collected, followed by euthanasia via cervical dislocation. Serum was subsequently separated from the blood samples. The study protocol was approved by the Research Ethics Committee of The Fourth Hospital of Hebei Medical University (Approval No. 2022KY257). All experiments were conducted in accordance with the ethical standards of the Declaration of Helsinki (Approval No. IACUC-4th Hos Hebmu).

Terminal deoxynucleotidyl transferase dUTP nick end labeling (TUNEL) staining

The mouse tumor tissues were fixed with 4% paraformaldehyde for 24 hours, then embedded in paraffin and serially sectioned (4 μm). Subsequently, the tissues were fully deparaffinized with xylene (X821391, Macklin) and rehydrated using a graded ethanol series. The sections were incubated with DNase-free proteinase K (20 μg/mL, HY-108717A, MedChemExpress) at 37°C for 15 min. TUNEL assay solution (C1086, Beyotime) was added, and the sections were incubated for 60 minutes in the dark. Then, the sections were stained with DAPI solution (C1006, Beyotime) in the dark for 10 min to label cell nuclei, followed by visualization and imaging under a fluorescence microscope.

$CD8^+$ T cell marker detection

Fresh tumor tissue from mice was collected and minced into small pieces (approximately 1 mm^3) using sterile scissors. The minced tissue was incubated in digestion buffer containing collagenase IV (1 mg/mL, HY-E70005D, MedChemExpress) and DNase I (30 μg/mL, D7076, Beyotime) for 40 minutes at 37°C with gentle shaking. The tissue was gently dissociated by pipetting every 10 minutes to fully disperse the tissue into single cells. The tissue fragments were removed by filtering the sample through a 70 μm cell strainer. The filtrate was centrifuged, and the pellet was resuspended in PBS to prepare a single-cell suspension (1.0×10^7 cells/mL). An appropriate volume of single-cell suspension was added to a flow tube, and CD3 antibody (11-0032-82, Invitrogen) and CD8 antibody (MA1-145, Invitrogen) were added and mixed by gentle pipetting. After incubation for 30 min in the dark, cells were rinsed with PBS, analyzed using flow cytometry, and $CD8^+$ T cell infiltration was evaluated using FlowJo v10.8 software [21].

Enzyme-linked immunosorbent assay (ELISA)

Mouse $CD8^+$ T cell activation was assessed using ELISA kits for IFN-γ (PI508, Beyotime),

TNF-α (PT512, Beyotime), perforin (JL23590-48T, JonInbio Industrial Co., Ltd., Shanghai, China), and granzyme B (ab238265, Abcam). Then, 100 μL of mouse serum was added to each well of the ELISA plate, and the plate was incubated for 2 hours at 25°C. Subsequently, 100 μL of the corresponding biotin-labeled antibody was added to each well and with incubated for 1 hour. After washing with PBS, 100 μL of horseradish peroxidase-labeled streptavidin solution was added and incubated for 20 minutes. TMB color developer solution was added according to the manufacturer's instructions, followed by a 10-minute incubation at 37°C in the dark. Then, 50 μL of stop solution was added and mixed gently. The OD450 values were determined using a microplate reader.

Western blot

Mouse tumor tissues were cut into pieces, mixed with radioimmunoprecipitation assay lysis buffer (P0013B, Beyotime), and homogenized. After transfection with different plasmids, TE1 cells were gently rinsed with PBS and then fully lysed with radioimmunoprecipitation assay lysis buffer. The supernatant was collected by centrifugation, and the protein concentration was determined using a bicinchoninic acid assay. The protein samples were mixed with SDS-PAGE protein loading buffer and then boiled for 8 minutes. After SDS-PAGE, proteins were transferred to a polyvinylidene difluoride membrane (Invitrogen) and blocked with 5% bovine serum albumin (BSA, A801320, Macklin) for 90 minutes [22]. Subsequently, the membranes were incubated with primary antibodies overnight at 4°C. After rinsing with Tris-buffered saline with Tween 20, the membranes were incubated with goat anti-rabbit IgG (32460, 1:500, Invitrogen) for 1 hour at 25°C. Antibodies were diluted in 5% BSA solution. The enhanced chemiluminescence working solution (E917968, Macklin) was applied evenly to the membrane surface, incubated for 1 minute, and then scanned using a JP-2880 gel imaging system (Jinpeng Analysis Instrument Co., Ltd., Shanghai, China). Using GAPDH (PA1-988, 1:5000, Invitrogen) as an internal control, the gray values were quantified using ImageJ software.

The primary antibodies used were: LAMP5 (PA5-52112, 1:2000, Invitrogen), Ki-67 (ab-16667, 1:5000, Abcam), cleaved caspase-3 (ab214430, 1:5000, Abcam), proliferating cell nuclear antigen (PA5-27214, 1:2000, Invitrogen), caspase-3 (ab32351, 1:5000, Abcam), B-cell lymphoma 2 (Bcl-2)-associated X protein (MA5-35342, 1:2000, Invitrogen), and Bcl-2 (ab194583, 1:500, Abcam).

Immunohistochemistry (IHC)

IHC staining was performed using a protocol described previously [23]. Paraffin-embedded sections were dewaxed in xylene baths and then rehydrated using a graded ethanol series. The sections were incubated with the primary antibody against LAMP5 (PA5-52112, 1:1000, Invitrogen) overnight at 4°C. A pathologist blinded to clinical data scored the LAMP5-stained sections using an optical microscope. IHC results were expressed as LAMP5 positivity scores, with higher scores indicating higher levels of expression.

In addition, paraffin sections of tumor tissue were deparaffinized and rehydrated using a graded ethanol series. Subsequently, sections were subjected to antigen retrieval by microwave in citrate buffer (pH 6.0) and then immersed in 3% H_2O_2 solution for 30 minutes. Sections were blocked with 5% BSA for 30 minutes. Then, they were incubated with primary antibody against Ki-67 (ab16667, 1:500, Abcam) overnight at 4°C, followed by incubation with goat anti-rabbit IgG at 37°C for 30 minutes. 3,3'-diaminobenzidine (P0203, Beyotime) was used for the chromogenic reaction, and the color development was terminated by rinsing with distilled water after approximately 15 minutes. The cell nuclei were stained with hematoxylin solution (HY-N0116, MedChemExpress), and the samples were then observed under an optical microscope.

Immunofluorescence

Paraffin sections were dewaxed using xylene and rehydrated using a graded ethanol series. Then, 0.3% Triton X-100 (T824275, Macklin) was applied to the sections for 10 minutes to permeabilize the cells. After blocking with 5% BSA for 60 minutes, the sections were incubated with primary antibody against CD8 (MA1-145, 1:20, Invitrogen) at 4°C for 12 hours. Then, the sections were incubated with goat anti-rat IgG (A-11006, 1:250, Invitrogen) for 90

minutes in the dark and then observed under a fluorescence microscope.

TE1 cells were seeded into 12-well plates (2×10^5 cells/well). At 48 hours after transfection with different plasmids, the cells were fixed with 4% paraformaldehyde for 30 minutes. After incubation with 0.3% Triton X-100 for 10 minutes and blocking with 5% BSA for 1 hour, the cells were incubated with primary antibody against LAMP5 (50-9778-80, 1:100, Invitrogen) overnight at 4°C. The remaining procedures were the same as the immunofluorescence staining steps for tumor tissue sections described above.

Immune cell infiltration estimated by CIBERSORT method

The proportions of 22 immune cell types in each ESCC patient sample were quantified using the CIBERSORT method [24], a deconvolution algorithm for gene expression profiles. The LM22 signature matrix and the CIBERSORT.R were obtained from the following websites: https://content.cruk.cam.ac.uk/fmlab/sivakumar2016/LM22.txt and https://content.cruk.cam.ac.uk/fmlab/sivakumar2016/Cibersort.R. Samples with low confidence (P>0.05) were excluded from further analysis. The immune cell proportions in normal and ESCC samples were determined using R software.

Statistical analysis

In the present study, all statistical analyses were performed using R software (version 4.1.1). All experimental data were also analyzed using SPSS software (version 25.0). For comparisons between two groups, the statistical significance of normally distributed variables was analyzed using the Student's t-test (results are expressed as mean ± standard deviation), while non-normally distributed variables were analyzed using the Wilcoxon test. For paired comparisons between cancerous tissues and adjacent normal tissues from the same patient, a paired Student's t-test was used. For comparisons among multiple independent groups, one-way analysis of variance followed by Tukey's post-hoc test was performed; for data analysis at multiple time points (tumor volume), repeated-measures analysis of variance was used with Bonferroni's post-hoc test. Survival differences were evaluated using the log-rank test. Each experiment was performed at least three times, A p-value <0.05 was considered statistically significant.

Results

Screening of DEGs and functional enrichment analysis in ESCC

We used the GSE53624 and GSE32424 datasets to screen DEGs. There were 830 DEGs in the GSE53624 dataset, comprising 246 upregulated genes and 584 downregulated expression (**Figure 1A** and **1B**). In the GSE32424 dataset, 1,731 genes were upregulated and 862 were downregulated (**Figure 1C** and **1D**). In addition, the expression profiles of DEGs in GSE32424 and GSE53624 were visualized using volcano plots and heatmaps. Among these, 470 DEGs overlapped between the GSE53624 and GSE32424 datasets (**Figure 1E**). To elucidate the functions of the common DEGs, GO, KEGG, and GSEA were performed. The biological process terms were enriched in external encapsulating structure organization, extracellular matrix (ECM)/structure organization, epidermal cell differentiation, and leukocyte migration/chemotaxis. The cellular component terms were enriched in ECM, fibrillar collagen trimer, and basement membrane. The molecular function terms were enriched in ECM structural constituent, cytokine activity, and growth factor binding (**Figure 1F**). KEGG pathway enrichment analysis revealed enrichment in arachidonic acid metabolism, ECM-receptor interaction, and focal adhesion (**Figure 1G**). GSEA further demonstrated that the DEGs were predominantly enriched in the epithelial-mesenchymal transition (EMT) pathway (**Figure 1H**). These results indicated that the common DEGs are mainly involved in ECM remodeling, cell differentiation, adhesion, and EMT, which may contribute to the malignant progression of ESCC.

Development and validation of a four-gene prognostic signature for ESCC

To explore the association between DEGs and prognostic characteristics in ESCC, a univariate cox regression analysis based on GSE53624 was performed. The results showed that 17 DEGs were associated with OS (**Table 2**). LASSO regression analysis was then

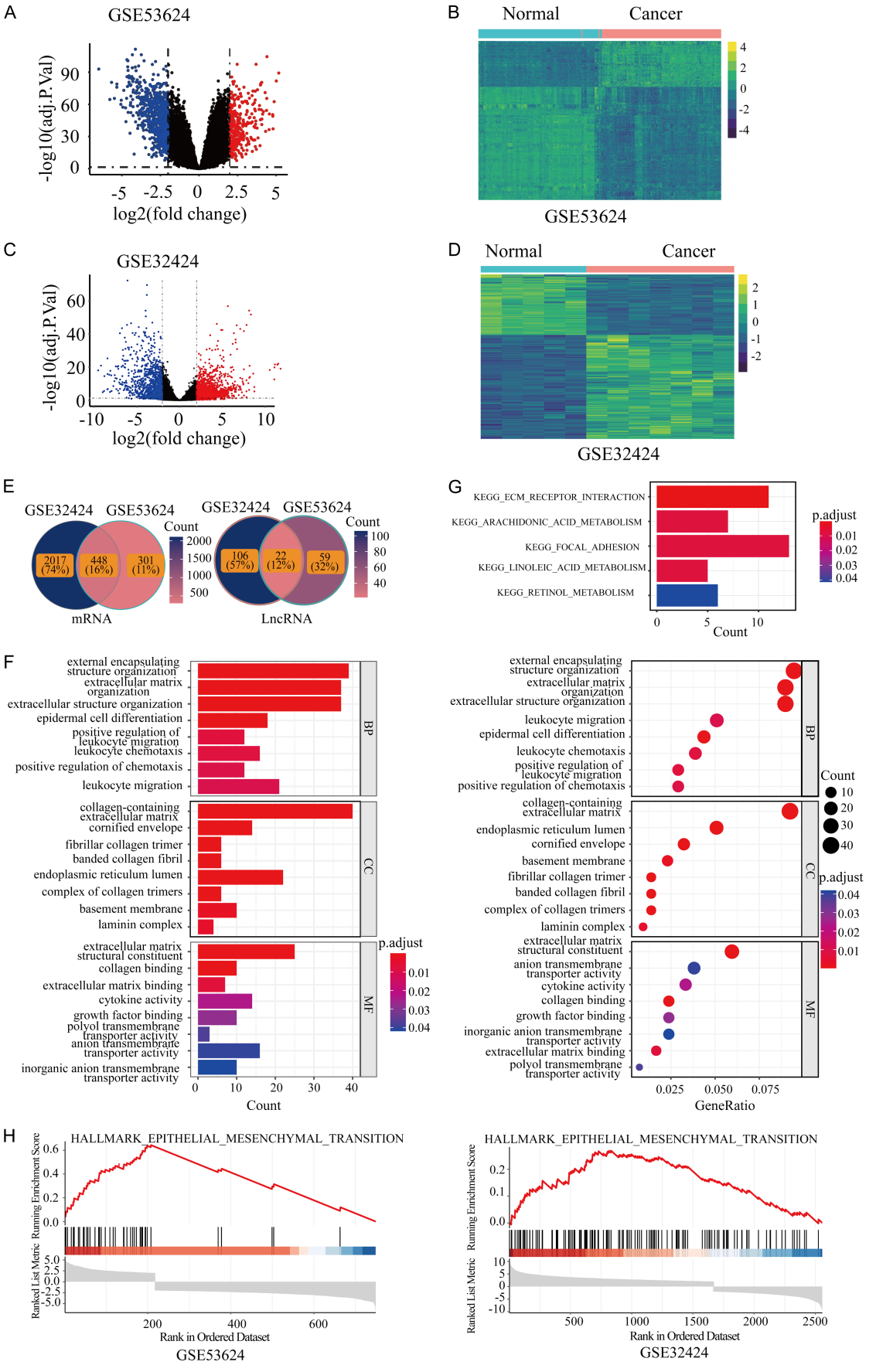
A
GSE53624
-log10(adj.P.Val)
log2(fold change)
B
Normal
Cancer
GSE53624
C
GSE32424
-log10(adj.P.Val)
log2(fold change)
D
Normal
Cancer
GSE32424
E
GSE32424
GSE53624
2017 (74%)
448 (16%)
301 (11%)
mRNA
106 (57%)
22 (12%)
59 (32%)
LncRNA
Count
G
KEGG_ECM_RECEPTOR_INTERACTION
KEGG_ARACHIDONIC_ACID_METABOLISM
KEGG_FOCAL_ADHESION
KEGG_LINOLEIC_ACID_METABOLISM
KEGG_RETINOL_METABOLISM
p.adjust
Count
F
external encapsulating structure organization
extracellular matrix organization
extracellular structure organization
epidermal cell differentiation
positive regulation of leukocyte migration
leukocyte chemotaxis
positive regulation of chemotaxis
leukocyte migration
collagen-containing extracellular matrix
cornified envelope
fibrillar collagen trimer
banded collagen fibril
endoplasmic reticulum lumen
complex of collagen trimers
basement membrane
laminin complex
extracellular matrix structural constituent
collagen binding
extracellular matrix binding
cytokine activity
growth factor binding
polyol transmembrane transporter activity
anion transmembrane transporter activity
inorganic anion transmembrane transporter activity
BP
CC
MF
p.adjust
Count
GeneRatio
H
HALLMARK_EPITHELIAL_MESENCHYMAL_TRANSITION
Running Enrichment Score
Ranked List Metric
Rank in Ordered Dataset
GSE53624
GSE32424

Figure 1. Screening of DEGs and functional enrichment analysis in ESCC. A. Volcano plot of the DEGs in the GSE53624 dataset (red dots indicate upregulated DEGs; blue dots indicate downregulated DEGs). B. Heatmap of the DEGs in the GSE53624 dataset. C. Volcano plot of the DEGs in the GSE32424 dataset. D. Heatmap of the DEGs in the GSE32424 dataset. E. DEGs were identified from the GSE53624 and GSE32424 datasets ($P<0.05$ and $|logFC|\geq2$), yielding a total of 470 overlapping genes. F. GO analysis of the 470 overlapping DEGs, including biological process, cellular component, and molecular function terms. G. KEGG pathway analysis of the 470 DEGs. H. GSEA of the 470 overlapping DEGs using the hallmark gene set. DEGs: Differentially expressed genes; ESCC: Esophageal squamous cell carcinoma; GO: Gene ontology; KEGG: Kyoto encyclopedia of genes and genomes; GSEA: Gene set enrichment analysis.

Table 2. The 17 genes associated with prognosis of ESCC

Gene	HR	95% CI	*p*-value
COL22A1	1.12	(1.01-1.25)	0.036
LAMP5	1.19	(1.03-1.38)	0.022
PLAU	1.75	(1.22-2.52)	0.002
SCG2	1.19	(1.01-1.4)	0.034
CLDN7	0.82	(0.69-0.98)	0.032
EPS8L1	0.76	(0.59-0.97)	0.027
GRHL3	0.78	(0.66-0.92)	0.004
LIPH	0.81	(0.68-0.98)	0.026
MUC15	0.86	(0.76-0.98)	0.021
RAB25	0.68	(0.54-0.84)	0.001
SLPI	0.84	(0.72-0.97)	0.015
VSIG2	0.75	(0.57-0.99)	0.040
CNN1	1.38	(1.07-1.78)	0.012
CRYBG2	0.73	(0.55-0.99)	0.039
LMOD1	1.23	(1.01-1.5)	0.038
MPZL3	0.68	(0.51-0.90)	0.008
THSD4	1.27	(1.01-1.59)	0.042

ESCC: Esophageal squamous cell carcinoma; HR: Hazard ratio; CI: Confidence interval; COL22A1: Collagen type XXII alpha 1 chain; LAMP5: Lysosomal-associated membrane protein 5; PLAU: Urokinase-type plasminogen activator; SCG2: Secretogranin II; CLDN7: Claudin 7; EPS8L1: EPS8-like 1; GRHL3: Grainyhead-like transcription factor 3; LIPH: Lipase H; MUC15: Mucin 15; RAB25: RAS-related protein 25; SLPI: Secretory leukocyte peptidase inhibitor; VSIG2: V-set and immunoglobulin domain containing 2; CNN1: Calponin 1; CRYBG2: Crystallin beta-gamma domain containing 2; LMOD1: Leiomodin 1; MPZL3: Myelin protein zero-like 3; THSD4: Thrombospondin type 1 domain containing 4.

applied to further filter genes from the 17 survival-related genes (**Figure 2A** and **2B**), and four genes were selected: GRHL3, LAMP5, PLAU, and RAB25. Next, we explored the relationship between the four genes and survival outcomes in ESCC patients with respect to key clinicopathological characteristics. GRHL3 and RAB25 were favorable prognostic factors for age, gender, tumor stage, and lymph node metastasis, while RAB25 was also favorable for clinical stage. LAMP5 and PLAU were associated with poorer prognosis for gender, lymph node metastasis, and clinical stage; PLAU was additionally associated with poorer prognosis for tumor stage and age (**Figure 2C**). Thus, the four genes were correlated with clinicopathologic parameters in ESCC patients.

We conducted multivariate Cox regression analysis on the four identified genes to develop a prognostic model for ESCC patients, and the model exhibited statistical significance ($P<0.01$, **Figure 2D**). Compared with other genes, LAMP5 might serve as an independent prognostic factor. On the basis of this analysis, we obtained the coefficients of the four genes to calculate the risk score as follows: Risk score = (-0.12 × GRHL3 level) + (-0.23 × RAB25 level) + (0.15 × LAMP5 level) + (0.33 × PLAU level). The risk scores of patients in the deceased group were considerably higher than those in the surviving group (**Figure 2E**). Patients were categorized into high-risk and low-risk groups using the median risk score (1.80) as the cutoff. The OS was shorter in the high-risk group (**Figure 2F**). The area under the curve (AUC) was 0.695, and the optimal risk score cutoff value was determined to be 1.87. The risk score distributions, OS status, and expression heatmap of the four genes in each patient are shown in **Figure 2G**. In addition, time-dependent ROC curves were generated to evaluate 1-, 3-, and 5-year OS predictions. The AUCs were 0.705, 0.742, and 0.709, respectively (**Figure 2H**). These findings demonstrated that the four-gene risk signature might be capable of evaluating the prognosis of ESCC.

Construction and validation of the prognostic nomogram and clinical tissue verification in ESCC

To evaluate the correlation between the risk signature and clinicopathological characteristics in predicting the prognosis of ESCC, Cox

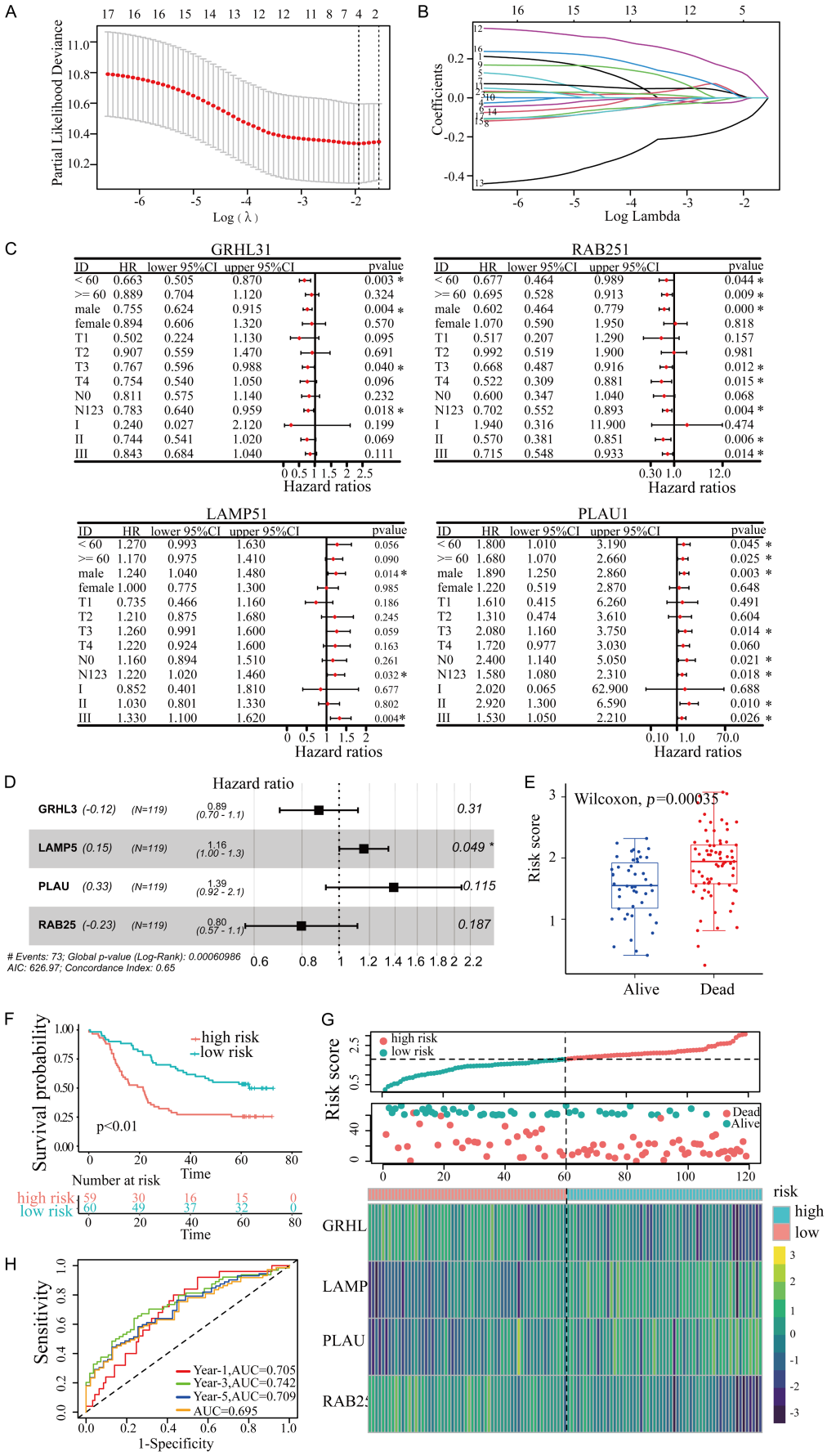
A
Partial Likelihood Deviance
Log (λ)
B
Coefficients
Log Lambda
C
GRHL31
ID HR lower 95%CI upper 95%CI pvalue
< 60 0.663 0.505 0.870 0.003 *
>= 60 0.889 0.704 1.120 0.324
male 0.755 0.624 0.915 0.004 *
female 0.894 0.606 1.320 0.570
T1 0.502 0.224 1.130 0.095
T2 0.907 0.559 1.470 0.691
T3 0.767 0.596 0.988 0.040 *
T4 0.754 0.540 1.050 0.096
N0 0.811 0.575 1.140 0.232
N123 0.783 0.640 0.959 0.018 *
I 0.240 0.027 2.120 0.199
II 0.744 0.541 1.020 0.069
III 0.843 0.684 1.040 0.111
Hazard ratios
RAB251
ID HR lower 95%CI upper 95%CI pvalue
< 60 0.677 0.464 0.989 0.044 *
>= 60 0.695 0.528 0.913 0.009 *
male 0.602 0.464 0.779 0.000 *
female 1.070 0.590 1.950 0.818
T1 0.517 0.207 1.290 0.157
T2 0.992 0.519 1.900 0.981
T3 0.668 0.487 0.916 0.012 *
T4 0.522 0.309 0.881 0.015 *
N0 0.600 0.347 1.040 0.068
N123 0.702 0.552 0.893 0.004 *
I 1.940 0.316 11.900 0.474
II 0.570 0.381 0.851 0.006 *
III 0.715 0.548 0.933 0.014 *
Hazard ratios
LAMP51
ID HR lower 95%CI upper 95%CI pvalue
< 60 1.270 0.993 1.630 0.056
>= 60 1.170 0.975 1.410 0.090
male 1.240 1.040 1.480 0.014 *
female 1.000 0.775 1.300 0.985
T1 0.735 0.466 1.160 0.186
T2 1.210 0.875 1.680 0.245
T3 1.260 0.991 1.600 0.059
T4 1.220 0.924 1.600 0.163
N0 1.160 0.894 1.510 0.261
N123 1.220 1.020 1.460 0.032 *
I 0.852 0.401 1.810 0.677
II 1.030 0.801 1.330 0.802
III 1.330 1.100 1.620 0.004*
Hazard ratios
PLAU1
ID HR lower 95%CI upper 95%CI pvalue
< 60 1.800 1.010 3.190 0.045 *
>= 60 1.680 1.070 2.660 0.025 *
male 1.890 1.250 2.860 0.003 *
female 1.220 0.519 2.870 0.648
T1 1.610 0.415 6.260 0.491
T2 1.310 0.474 3.610 0.604
T3 2.080 1.160 3.750 0.014 *
T4 1.720 0.977 3.030 0.060
N0 2.400 1.140 5.050 0.021 *
N123 1.580 1.080 2.310 0.018 *
I 2.020 0.065 62.900 0.688
II 2.920 1.300 6.590 0.010 *
III 1.530 1.050 2.210 0.026 *
Hazard ratios
D
Hazard ratio
GRHL3 (-0.12) (N=119) 0.89 (0.70 - 1.1) 0.31
LAMP5 (0.15) (N=119) 1.16 (1.00 - 1.3) 0.049 *
PLAU (0.33) (N=119) 1.39 (0.92 - 2.1) 0.115
RAB25 (-0.23) (N=119) 0.80 (0.57 - 1.1) 0.187
Events: 73; Global p-value (Log-Rank): 0.00060986
AIC: 626.97; Concordance Index: 0.65
E
Wilcoxon, p=0.00035
Risk score
Alive
Dead
F
Survival probability
high risk
low risk
p<0.01
Number at risk
high risk 59 30 16 15 0
low risk 60 49 37 32 0
Time
G
Risk score
high risk
low risk
Dead
Alive
GRHL
LAMP
PLAU
RAB2
risk
high
low
H
Sensitivity
1-Specificity
Year-1,AUC=0.705
Year-3,AUC=0.742
Year-5,AUC=0.709
AUC=0.695

Figure 2. Development and validation of a four-gene prognostic signature for ESCC. A. Partial likelihood deviance for optimizing parameter selection in the LASSO regression model for the GSE53624 dataset. B. LASSO coefficient profiles of the 17 DEGs. C. Forest plots of the four prognostic DEGs identified using univariate Cox regression for clinicopathological characteristics of ESCC patients. D. Coefficients, HRs, and *p*-values for the four-gene signature obtained from multivariate Cox regression analysis. E. Risk scores deceased and surviving patients. F. Kaplan-Meier survival curves for OS of ESCC patients in low- and high-risk groups. G. Risk score distribution, OS status, and expression heatmap of the four prognostic genes in the GSE53624 dataset. H. Time-dependent ROC curves for the prognostic risk signature predicting 1-, 3-, and 5-year OS. ESCC: Esophageal squamous cell carcinoma; DEGs: Differentially expressed genes; OS: Overall survival; GRHL3: Grainyhead-like transcription factor 3; LAMP5: Lysosomal-associated membrane protein 5; RAB25: RAS-related protein 25; PLAU: Urokinase-type plasminogen activator; ID: Identifier; HR: Hazard ratio; CI: Confidence interval; T1: Tumor stage 1; T2: Tumor stage 2; T3: Tumor stage 3; T4: Tumor stage 4; N0: Node stage 0; N123: Node stage 1, 2, 3; I: Stage I; II: Stage II; III: Stage III; LASSO: Least absolute shrinkage and selection operator; ROC: Receiver operating characteristic; AUC: Area under the curve. **P*<0.05.

regression analysis was performed. For ESCC patients, univariate analysis identified N stage, TNM stage, and the risk score as significant risk factors for OS. Multivariate analysis further demonstrated that the risk score was an independent prognostic factor for ESCC (**Figure 3A** and **3B**). Next, we established a clinical nomogram model based on N stage, TNM stage, and risk stratification to predict the 1-, 3-, and 5-year OS rates of ESCC patients (**Figure 3C**). Furthermore, time-dependent ROC curve analysis of the nomogram model showed that the AUCs were 0.620, 0.769, and 0.743 for predicting 1-, 3-, and 5-year OS, respectively, with an overall AUC of 0.746 (**Figure 3D**). Calibration curves of the nomogram model were established to assess its predictive value, demonstrating that the predicted survival rates for ESCC patients aligned with their actual survival outcomes (**Figure 3E**). To enhance the reliability of the bioinformatic analyses, qRT-PCR results showed that GRHL3 and RAB25 mRNA levels were significantly downregulated in 65 pairs of ESCC cancer tissues compared with normal tissues, whereas LAMP5 and PLAU were significantly upregulated in ESCC tissues (**Figure 3F**). Furthermore, we calculated the risk scores for 65 ESCC patients based on the coefficients of the four genes. Patients who died had higher risk scores than those who survived (**Figure 3G**). OS was significantly shorter in the high-risk group, with an AUC of 0.780 (**Figure 3H** and **3I**). To assess the prognostic potential of the four candidate genes in survival risk prediction, ROC analysis was performed. LAMP5 emerged as the most robust predictor, demonstrating superior discriminative capacity in risk stratification (AUC = 0.773, **Figure 3J**). The findings from bioinformatic analysis aligned with these results. However, there have been no prior reports concerning the expression and function of LAMP5 in ESCC. In addition, IHC was performed to analyze LAMP5 protein expression in both ESCC and normal tissues. Notably, LAMP5 displayed higher expression in ESCC tissues (**Figure 3K**). Correlation analysis revealed that high LAMP5 expression was significantly correlated with tumor differentiation, T stage, TNM stage, and lymph node metastasis, but not with patient age or gender (**Table 3**). These results suggest that LAMP5 may contribute to the tumorigenesis and progression of ESCC.

Overexpression of LAMP5 promotes proliferation and inhibits apoptosis in ESCC cells

LAMP5 mRNA expression was higher in ESCC cells than that in control cells (**Figure 4A**). Among these cell lines, LAMP5 exhibited the lowest expression level in TE1 cells; therefore, we chose this cell line for subsequent assays. To explore the regulatory role of LAMP5 in the malignant phenotype of ESCC cells, we transfected pcDNA3.1/pcDNA3.1-LAMP5 and si-NC/si-LAMP5 into TE1 cells. Transfection of pcDNA3.1-LAMP5 significantly upregulated LAMP5 mRNA levels in cells, whereas transfection of si-LAMP5 effectively reduced LAMP5 expression, indicating successful overexpression and knockdown of LAMP5 (**Figure 4B**). Immunofluorescence results showed that LAMP5 overexpression significantly increased LAMP5 fluorescence intensity, and LAMP5 was localized to the cell membrane, whereas LAMP5 knockdown had the opposite effect (**Figure 4C**). Transfection of pcDNA3.1-LAMP5 significantly increased TE1 cell viability, while transfection of si-LAMP5 had an inhibitory effect on cell viability (**Figure 4D**). In addition, LAMP5 overexpression significantly increased colony formation (**Figure 4E**) and promoted

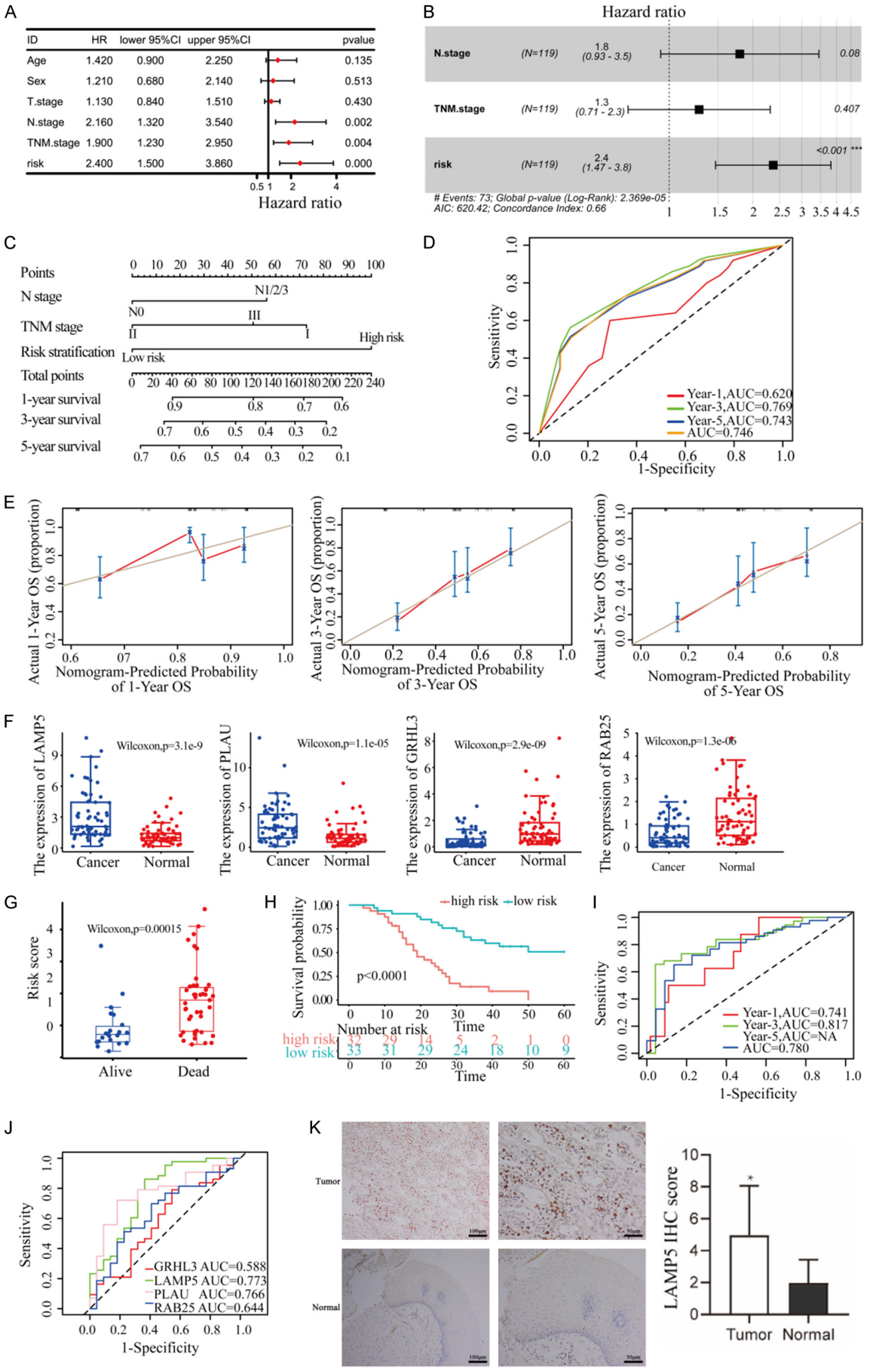
A
ID HR lower 95%CI upper 95%CI pvalue
Age 1.420 0.900 2.250 0.135
Sex 1.210 0.680 2.140 0.513
T.stage 1.130 0.840 1.510 0.430
N.stage 2.160 1.320 3.540 0.002
TNM.stage 1.900 1.230 2.950 0.004
risk 2.400 1.500 3.860 0.000
Hazard ratio
B
Hazard ratio
N.stage (N=119) 1.8 (0.93 - 3.5) 0.08
TNM.stage (N=119) 1.3 (0.71 - 2.3) 0.407
risk (N=119) 2.4 (1.47 - 3.8) <0.001 ***
Events: 73; Global p-value (Log-Rank): 2.369e-05
AIC: 620.42; Concordance Index: 0.66
C
Points
N stage
TNM stage
Risk stratification
Total points
1-year survival
3-year survival
5-year survival
N1/2/3
N0
III
II
I
High risk
Low risk
D
Sensitivity
1-Specificity
Year-1,AUC=0.620
Year-3,AUC=0.769
Year-5,AUC=0.743
AUC=0.746
E
Actual 1-Year OS (proportion)
Nomogram-Predicted Probability of 1-Year OS
Actual 3-Year OS (proportion)
Nomogram-Predicted Probability of 3-Year OS
Actual 5-Year OS (proportion)
Nomogram-Predicted Probability of 5-Year OS
F
The expression of LAMP5
Wilcoxon,p=3.1e-9
The expression of PLAU
Wilcoxon,p=1.1e-05
The expression of GRHL3
Wilcoxon,p=2.9e-09
The expression of RAB25
Wilcoxon,p=1.3e-06
Cancer
Normal
G
Risk score
Wilcoxon,p=0.00015
Alive
Dead
H
high risk
low risk
Survival probability
p<0.0001
Number at risk
high risk 33 29 14 5 2 1 0
low risk 33 31 29 24 18 10 9
Time
I
Sensitivity
1-Specificity
Year-1,AUC=0.741
Year-3,AUC=0.817
Year-5,AUC=NA
AUC=0.780
J
Sensitivity
1-Specificity
GRHL3 AUC=0.588
LAMP5 AUC=0.773
PLAU AUC=0.766
RAB25 AUC=0.644
K
Tumor
Normal
LAMP5 IHC score
Tumor
Normal

Figure 3. Construction of the prognostic nomogram and clinical verification of LAMP5 in ESCC. A. Forest plot of univariate Cox regression analysis. B. Forest plot of multivariate Cox regression analysis for OS in ESCC patients based on clinicopathological characteristics and risk score. C. Nomogram combining N stage, TNM stage, and risk stratification for predicting 1-, 3-, and 5-year OS in ESCC patients. D. Time-dependent ROC curves of the nomogram model for predicting 1-, 3-, and 5-year OS in ESCC patients. E. Calibration curves of the nomogram showing the agreement between predicted and actual 1-, 3-, and 5-year OS in the GSE53624 dataset. F. qRT-PCR analysis of the four prognostic gene expression levels in 65 paired ESCC and normal tissues. G. Risk scores in deceased and surviving ESCC patients. H. Kaplan-Meier survival curves for OS in low-risk and high-risk ESCC patients. I. Time-dependent ROC curves of the prognostic risk signature for predicting 1- and 3-year OS in ESCC patients. J. ROC curves of the four genes for predicting OS in ESCC patients, demonstrating their prognostic sensitivity. K. LAMP5 protein expression in ESCC and normal tissues assessed by IHC (magnification: ×200 and ×400). ID: Identifier; HR: Hazard ratio; CI: Confidence interval; T stage: Tumor stage; N stage: Node stage; TNM stage: Tumor-node-metastasis stage; AUC: Aera under the curve; GRHL3: Grainyhead-like transcription factor 3; RAB25: RAS-related protein 25; PLAU: Urokinase-type plasminogen activator; LAMP5: Lysosomal associated membrane protein 5; ESCC: Esophageal squamous cell carcinoma; OS: Overall survival; qRT-PCR: Quantitative real-time PCR; ROC: Receiver operating characteristic; IHC: Immunohistochemistry; NA: Not applicable. *P<0.05, ***P<0.001.

Table 3. Correlation analysis of LAMP5 expression and clinicopathological characteristics in ESCC

Clinicopathologic parameters		Total (n)	LAMP5 expression		χ^2 *value*	*p-value*
			High	Low		
Age (years)	≥61	28	14	14	0.012	0.914
	<61	37	18	19		
Gender	Female	18	10	8	0.398	0.528
	Male	47	22	25		
Histological grade	G1+G2	45	18	27	4.986	0.026
	G3	20	14	6		
T-stage	T1+T2	16	4	12	10.211	0.001
	T3	49	28	21		
Lymph node metastasis	Yes	40	25	15	7.326	0.007
	No	25	7	18		
TNM stage	I+II	28	8	20	8.400	0.004
	III+IV	37	24	13		

ESCC: Esophageal squamous cell carcinoma; LAMP5: Lysosomal-associated membrane protein 5; TNM: Tumor-node-metastasis.

scratch wound healing (**Figure 4F**) in TE1 cells, whereas LAMP5 knockdown decreased colony formation and inhibited scratch wound healing. Transwell assay demonstrated that the number of invasive cells were significantly higher in the LAMP5 overexpression group and significantly lower in the LAMP5 knockdown group, suggesting that LAMP5 enhances the invasive ability of TE1 cells (**Figure 4G**). Furthermore, LAMP5 overexpression markedly decreased apoptosis rates, whereas LAMP5 knockdown increased apoptosis rates, indicating that LAMP5 inhibits apoptosis in TE1 cells (**Figure 4H**). Western blot demonstrated that LAMP5 overexpression notably increased Ki-67, Bcl-2, and proliferating cell nuclear antigen protein levels and decreased Bcl-2-associated X protein and cleaved caspase-3/caspase-3 protein levels, whereas LAMP5 knockdown reversed the expression levels of these proteins (**Figure 4I-K**). These results indicated that elevated LAMP5 expression is critically involved in ESCC progression.

LAMP5 suppresses CD8⁺ T cell activation and induces ESCC cell immune escape

To explore the impact of LAMP5 expression in ESCC cells on $CD8^+$ T cell activation, we co-cultured $CD8^+$ T cells with TE1 cells after transfection with different plasmids for 48 hours. CFSE staining results showed that co-culturing with LAMP5-overexpressing TE1 cells notably diminished the proportion of CFSE-positive $CD8^+$ T cells, whereas co-culturing with LAMP5-knockdown TE1 cells significantly increased CFSE-positive cells, suggesting that LAMP5 overexpression weakens the proliferative abili-

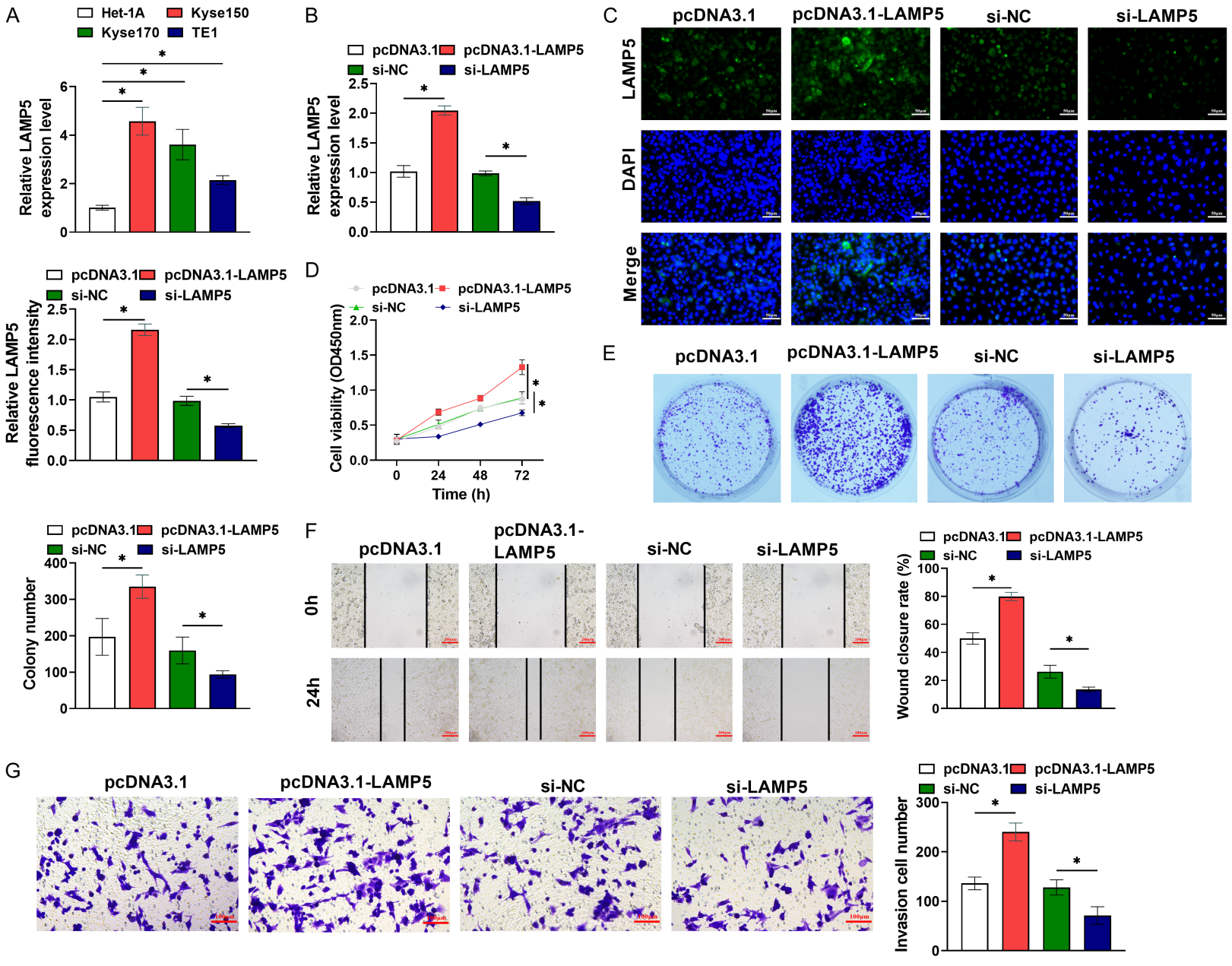
A
Het-1A
Kyse150
Kyse170
TE1
Relative LAMP5 expression level
B
pcDNA3.1
pcDNA3.1-LAMP5
si-NC
si-LAMP5
Relative LAMP5 expression level
C
pcDNA3.1
pcDNA3.1-LAMP5
si-NC
si-LAMP5
LAMP5
DAPI
Merge
D
Cell viability (OD450nm)
Time (h)
E
Colony number
F
0h
24h
Wound closure rate (%)
G
Invasion cell number

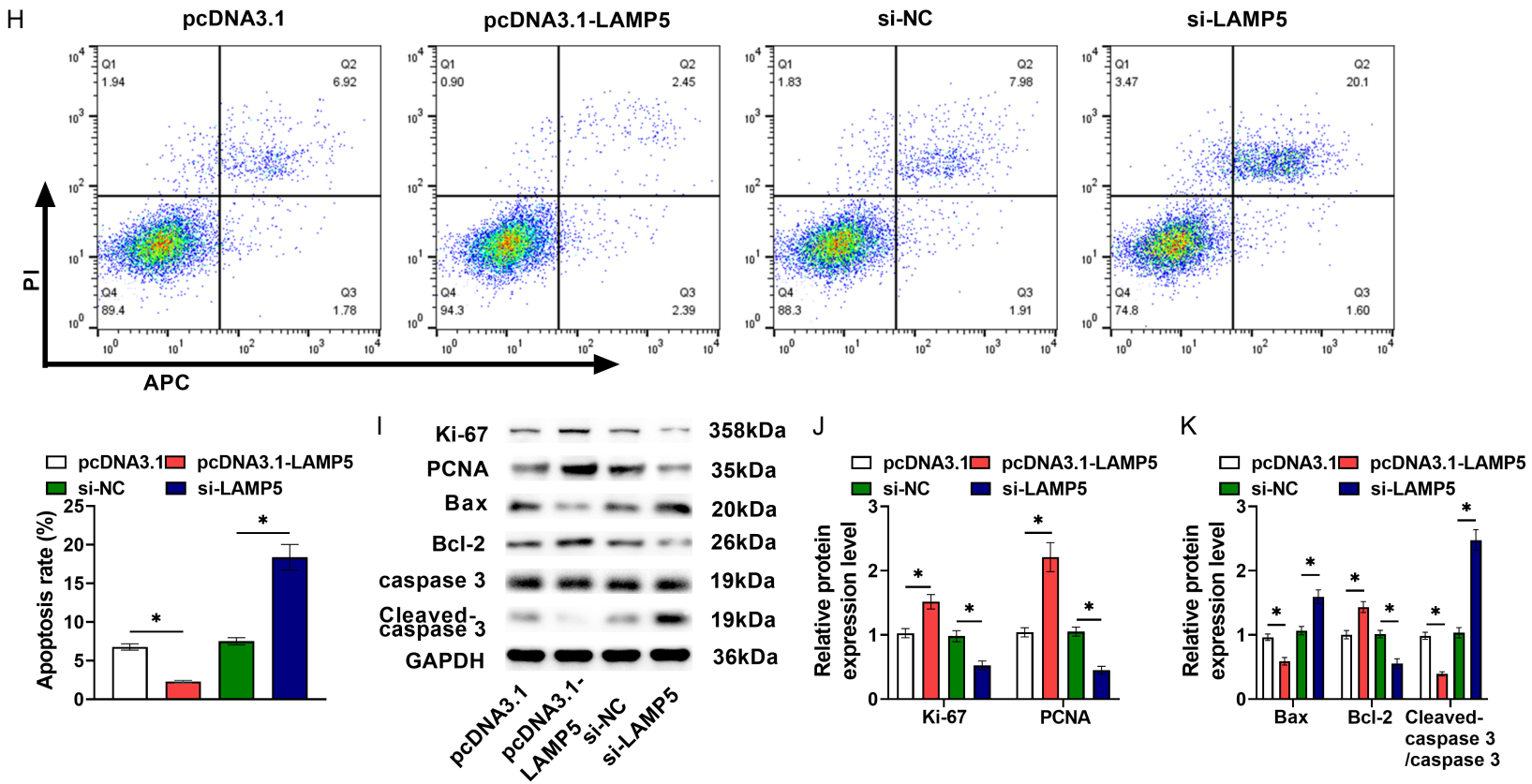

Figure 4. Overexpression of LAMP5 promotes proliferation and inhibits apoptosis in ESCC cells. A. LAMP5 expression was assessed using qRT-PCR in Het-1A cells and ESCC cell lines (Kyse150, Kyse170, and TE1). B. LAMP5 expression in TE1 cells after transfection with pcDNA3.1/pcDNA3.1-LAMP5 and si-NC/si-LAMP5. C. The subcellular localization of LAMP5 was detected by immunofluorescence (magnification: 40×). D. CCK-8 assay detected the viability of TE1 cells. E. Clone formation assay determined the number of clones formed in TE1 cells. F. Scratch assay was performed to assess the wound healing rate of transfected TE1 cells (magnification: 10×). G. Transwell assay assessed the invasive ability of TE1 cells (magnification: 20×). H. Flow cytometry determined the apoptosis of TE1 cells. I-K. Bax, Ki-67, Bcl-2, PCNA, caspase-3, and cleaved caspase-3 protein levels in TE1 cells were detected by Western blot. qRT-PCR: Quantitative real-time PCR; LAMP5: Lysosomal-associated membrane protein 5; ESCC: Esophageal squamous cell carcinoma; CCK-8: Cell counting kit-8; Bax: Bcl-2-associated X protein; Bcl-2: B-cell lymphoma 2; PCNA: Proliferating cell nuclear antigen; Het-1A: Human esophageal epithelial cell line (immortalized HET-1A, ATCC CRL-2692); KYSE150: Kyoto University esophageal squamous cell carcinoma cell line 150; KYSE170: Kyoto University esophageal squamous cell carcinoma cell line 170; TE1: Tohoku University esophageal squamous cell carcinoma cell line 1; pcDNA3.1: Plasmid Cytomegalovirus DNA 3.1 (empty vector control); pcDNA3.1-LAMP5: pcDNA3.1 vector expressing lysosomal-associated membrane protein 5; si-NC: Small interfering RNA negative control; si-LAMP5: Small interfering RNA targeting LAMP5; Ki-67: Ki-67 protein (named after Kiel, Germany and clone number 67); Merge: image channel merging (microscopy); DAPI 4',6-diamidino-2-phenylindole; OD450nm: Optical density at 450 nanometers; APC: Allophycocyanin; PI: Propidium iodide; GAPDH: Glyceraldehyde-3-phosphate dehydrogenase. *P<0.05.

ty of $CD8^+$ T cells (**Figure 5A**). Co-culturing with LAMP5-overexpressing TE1 cells markedly increased the apoptosis rate of $CD8^+$ T cells (**Figure 5B**) and decreased LDH release, reflecting reduced cytotoxicity (**Figure 5C**), whereas the LAMP5 knockdown group exhibited the opposite effect. In addition, LAMP5 overexpression notably deceased IFN-γ^+CD8^+ T cells, perforin$^+CD8^+$ T cells, granzyme B^+CD8^+ T cells, and TNF-α^+CD8^+ T cells, whereas LAMP5 knockdown remarkably elevated the percentages of these activated $CD8^+$ T cell subsets, indicating that LAMP5 overexpression effectively inhibits the activation of $CD8^+$ T cells (**Figure 5D-G**). Meanwhile, after co-culturing with $CD8^+$ T cells, TE1 cells transfected with pcDNA3.1-LAMP5 displayed a significant enhancement in cell viability, whereas si-LAMP5-transfected TE1 cells showed a notable reduction in viability, further confirming that LAMP5 overexpression weakens the cytotoxic effect of $CD8^+$ T cells on TE1 cells (**Figure 5H**). These results indicate that LAMP5 overexpression mediates immune escape of TE1 cells by suppressing $CD8^+$ T cell activation and reducing their killing function.

LAMP5-mediated immune cell infiltration and pathway enrichment analyses

Given the well-characterized association between immune cell infiltration and the immunotherapy response in cancer patients, we evaluated immune cell infiltration in ESCC patients using the CIBERSORT algorithm. Compared with normal tissues, $CD8^+$ T cells, and monocytes were reduced in cancer tissues. In contrast, macrophage M0 and macrophage M2 (in GSE32424), as well as resting NK cells, macrophage M0 and macrophage M1 (in GSE53624), showed higher proportions in cancer tissues. Additionally, in the GSE53624 dataset, activated NK cells and regulatory T cells showed lower proportions in cancer tissues (**Figure 6A** and **6B**). These results indicate that immune cells within the tumor tissue exhibit dysfunctional characteristics. Considering the aforementioned findings, we proposed that the low- and high-risk groups exhibit distinct immune microenvironment profiles. Furthermore, we observed an inverse relationship between LAMP5 expression and follicular helper T cells (Tfh) infiltration (**Figure 6C**). To investigate the potential mechanisms underlying LAMP5 in immune regulation, KEGG pathway enrichment analysis was performed on groups stratified by high and low LAMP5 expression. The results revealed marked enrichment of immune-related pathways, suggesting their potential roles in LAMP5-mediated immunomodulation (**Figure 6D**). These results suggest that LAMP5 may play a vital role in the immune microenvironment.

LAMP5 inhibits $CD8^+$ T cell activation in vivo and promotes tumor growth

To verify whether LAMP5 exerts a similar protumor effect *in vivo*, we established a mouse subcutaneous ESCC graft tumor model using mEC25 cells. LAMP5 expression and the proliferation marker Ki-67 were notably upregulated in the pcDNA3.1-LAMP5 group, whereas both were markedly reduced in the si-LAMP5 group (**Figure 7A**). LAMP5 overexpression significantly increased tumor volume and weight, whereas LAMP5 knockdown significantly inhibited tumor volume growth and decreased tumor weight (**Figure 7B-D**). IHC results further confirmed that the Ki-67 positive level was notably higher in the pcDNA3.1-LAMP5 group and notably lower in the si-LAMP5 group, suggesting that LAMP5 promotes tumor cell proliferation (**Figure 7E**). TUNEL-positive cells in tumor tissues were markedly decreased in the LAMP5 overexpression group and notably increased in the LAMP5 knockdown group, indicating that LAMP5 overexpression inhibits apoptosis of tumor cells (**Figure 7F**). Furthermore, CD8 fluorescence intensity (**Figure 7G**) and the proportion of $CD8^+$ T cell infiltration (**Figure 7H**) were notably reduced in the tumor tissues of the pcDNA3.1-LAMP5 group, whereas the si-LAMP5 group displayed the opposite pattern. TNF-α, IFN-γ, perforin, and granzyme B levels were notably reduced in the serum of the pcDNA3.1-LAMP5 group, whereas these $CD8^+$ T cell activation markers were markedly increased in the si-LAMP5 group (**Figure 7I**). These results confirm that LAMP5 overexpression promotes ESCC tumor growth and inhibits $CD8^+$ T cell activation in mice, whereas LAMP5 knockdown inhibits tumor progression and promotes $CD8^+$ T cell activation.

Discussion

We identified a total of 470 mRNAs that showed differential expression. Functional enrichment

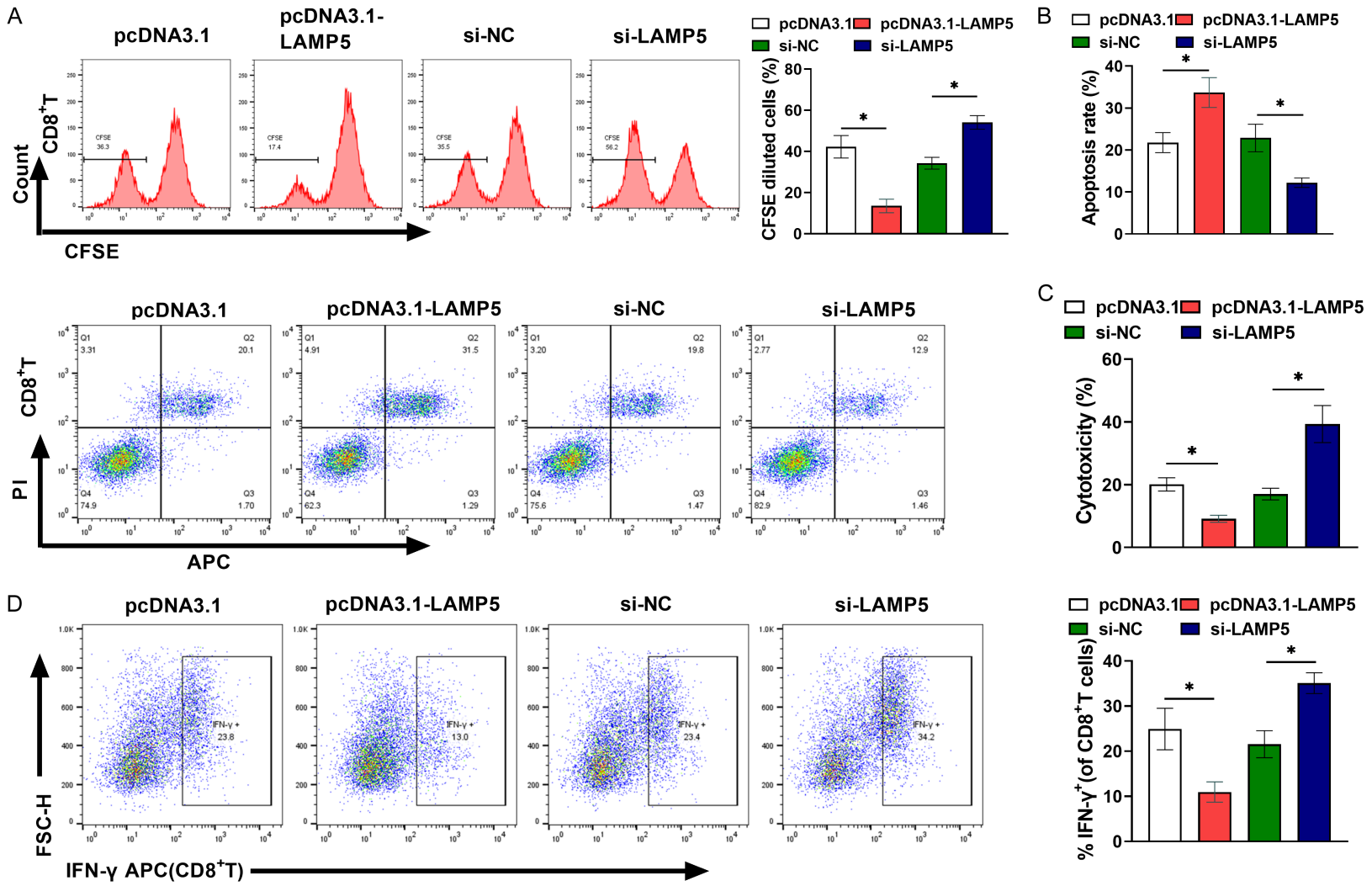
A
pcDNA3.1
pcDNA3.1-LAMP5
si-NC
si-LAMP5
Count
CD8+T
CFSE
CFSE diluted cells (%)
B
Apoptosis rate (%)
C
Cytotoxicity (%)
D
PI
APC
FSC-H
IFN-γ APC(CD8+T)
% IFN-γ+(of CD8+T cells)

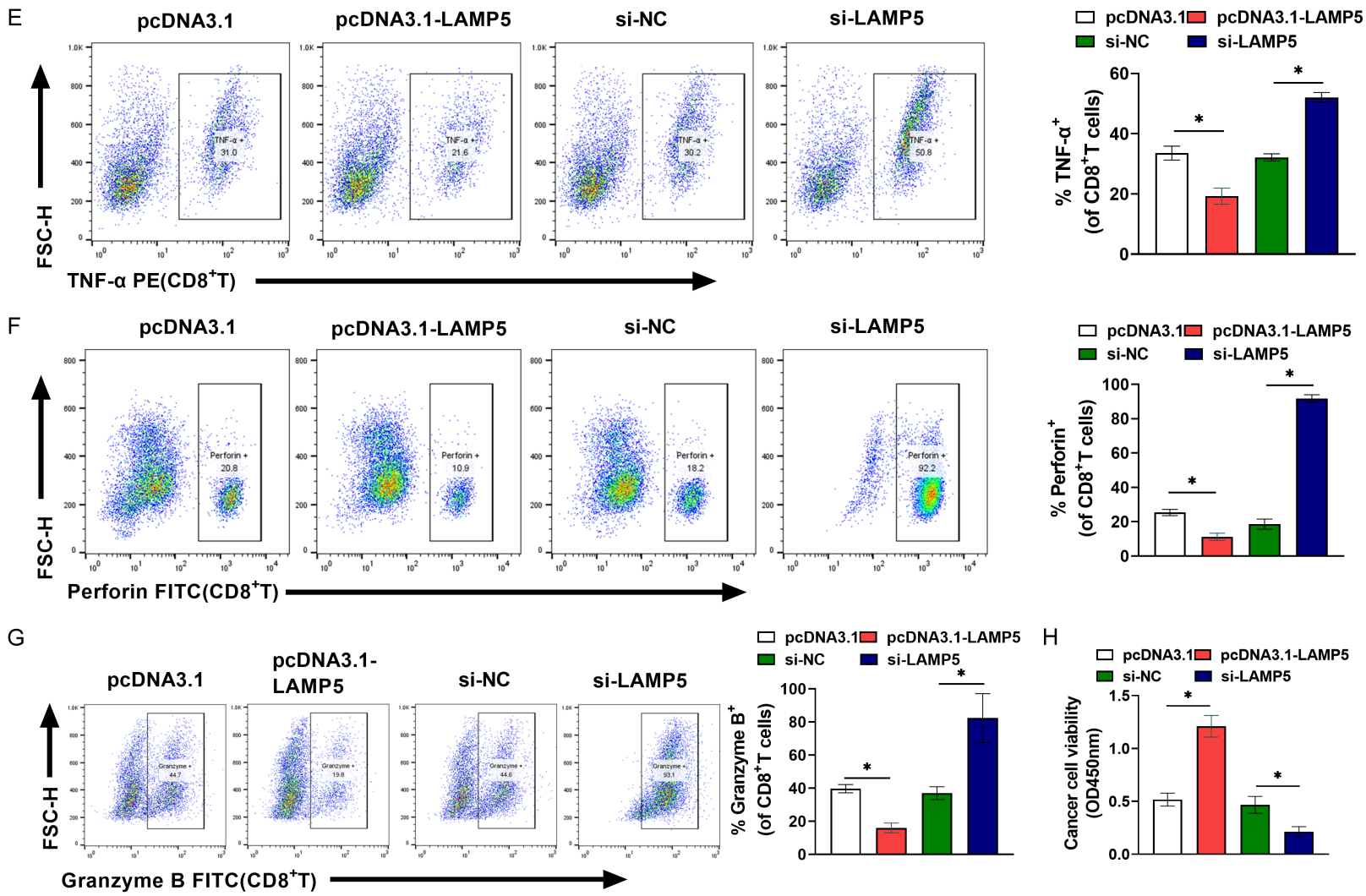

Figure 5. LAMP5 suppresses CD8+ T cell activation and induces ESCC cell immune escape. A. CD8+ T cells from healthy donors were isolated and co-cultured with LAMP5-overexpressing or LAMP5-knockdown TE1 cells for 48 hours. CFSE staining was used to detect the proliferative capacity of CD8+ T cells. B. Flow cytometry assessed the apoptosis rate of CD8+ T cells after co-culture with TE1 cells. C. After co-culture with TE1 cells, LDH release (reflecting cytotoxicity) was detected using an LDH assay kit. D-G. The proportions of CD8+ T cells positive for the activation markers IFN-γ, TNF-α, perforin, and granzyme B were detected by flow cytometry. H. The viability of TE1 cells was assessed using a CCK-8 assay. LAMP5: Lysosomal-associated membrane protein 5; ESCC: Esophageal squamous cell carcinoma; CFSE: Carboxyfluorescein succinimidyl ester; LDH: Lactate dehydrogenase; IFN-γ: Interferon-γ; TNF-α: Tumor necrosis factor-α; TE1: Tohoku University esophageal squamous cell carcinoma cell line 1; pcDNA3.1: Plasmid Cytomegalovirus DNA 3.1 (empty vector control); pcDNA3.1-LAMP5: pcDNA3.1 vector expressing lysosomal-

associated membrane protein 5; si-NC: Small interfering RNA negative control; si-LAMP5: Small interfering RNA targeting LAMP5; CCK-8: Cell counting kit-8; APC: Allophycocyanin; PI: Propidium iodide; OD450 nm: Optical density at 450 nanometers; $CD8^+$ T cells: Cluster of differentiation 8 positive T lymphocytes; FSC-H: Forward scatter height (flow cytometry); TNF-α PE: Tumor necrosis factor-alpha conjugated with phycoerythrin; Perforin FITC: Perforin conjugated with fluorescein isothiocyanate; Granzyme B FITC: Granzyme B conjugated with fluorescein isothiocyanate; Granzyme B^+: Granzyme B positive. *P<0.05.

analyses showed that these DEGs were mainly enriched in ECM/structure organization, epidermal cell differentiation, and leukocyte migration/chemotaxis at the GO level, and ECM-receptor interaction, focal adhesion at the KEGG pathway level. GSEA further verified the enrichment of the EMT pathway. These findings suggest that ECM, epidermal cell differentiation, cell adhesion, and EMT may play important roles in carcinogenesis of ESCC. It is worth noting that previous studies have also provided evidence supporting the significance of ECM, epidermal cell differentiation, cell adhesion, and EMT in tumorigenesis and cancer progression [25-28]. Additionally, cell adhesion, EMT, and leukocyte migration/chemotaxis have been associated with immune escape and metastasis of tumors [29-31].

Prognosis is a critical concern for cancer patients, and it is very important to explore prognosis-related genes for predicting the prognosis of various tumors [32, 33]. In our study, we identified four survival-related genes, including GRHL3, LAMP5, PLAU, and RAB25. Subsequently, we constructed a four-gene-based risk signature, which was identified to be linked with OS in ESCC patients. Additionally, we developed a nomogram integrating N stage, TNM stage, and risk score to predict the possibility of 1-, 3-, and 5-year OS for ESCC patients. This nomogram demonstrated superior accuracy in survival prediction. Similar approaches using nomograms have been employed in other cancer types, like pancreatic cancer and bladder cancer [34, 35]. The nomograms established in our study can potentially assist in the evaluation of survival outcomes for ESCC patients. Our study identified four genes (GRHL3, LAMP5, PLAU, and RAB25) as potential prognostic markers for ESCC. In particular, LAMP5 could be an independent prognostic factor.

GRHL3, PLAU and RAB25 have emerged as promising potential biomarkers for predicting the prognostic outcomes of ESCC patients. Prior studies demonstrated that GRHL3 had a vital function in tumorigenesis and the advancement of cancer [36]. PLAU exhibits aberrant overexpression in multiple tumor types and is crucial for tumor progression and metastasis. Specifically for ESCC, PLAU serves as a prognostic biomarker, effectively enhances the proliferative capability of tumor cells, and PLAU secreted by tumor cells was associated with the promotion of the development of inflammatory cancer-associated fibroblasts [37]. RAB25, exhibiting an epithelial distribution pattern, was first identified in normal gastrointestinal mucosa, kidney, and lung tissues [38]. As a complex molecular entity, it has been characterized as an intracellular transport protein. Tong *et al*. found Rab25 to function as a tumor suppressor in ESCC [39]. LAMP5 demonstrated overexpression in multiple myeloma as a lysosome membrane-associated protein [40]. Studies have confirmed that LAMP5 is linked to the proliferative activity of plasmacytoid dendritic cells (DCs) and participates in the immune tolerance system and also plays a critical role in tumorigenesis [41, 42]. Our study revealed that LAMP5 exhibits significant prognostic utility in evaluating patient outcomes. Furthermore, overexpression of LAMP5 increased proliferation, enhanced migration and invasion abilities, and inhibited apoptosis in TE1 cells. In the ESCC mouse model, overexpression of LAMP5 also promoted tumor growth and inhibited tumor cell apoptosis. Overall, this study further validated that LAMP5 may serve as a prognostic marker for ESCC.

Recently, growing evidence indicates that the TME plays a crucial part in tumor progression [43]. It is widely accepted that dysfunction of immune cells within TME results in evasion of the anti-tumor immune response of cancer cells, promoting tumor cell survival. The TME can maintain tumor-associated-macrophages in the functional state of immunosuppressive M2, leading to accelerated tumor progression [44, 45]. During tumorigenesis, $CD8^+$ T cells are known to differentiate into dysfunctional states and be induced by the immunosuppressive TME of established tumors [46-48]. NK cells play a critical role in immunosurveillance

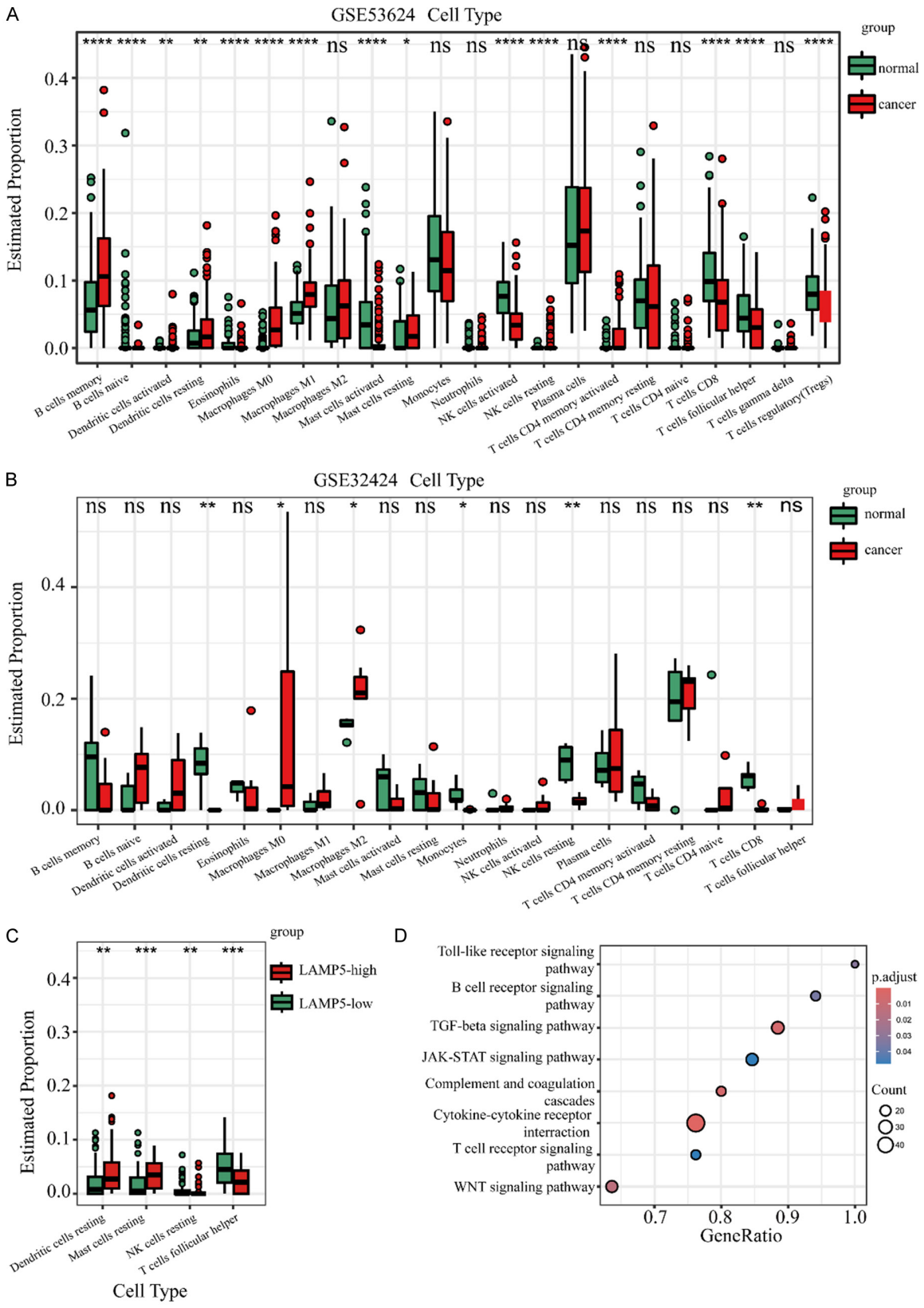

Figure 6. LAMP5-mediated immune cell infiltration and pathway enrichment analysis. A. Comparison of immune cell proportions between cancer and normal tissues in the GSE53624 dataset. B. Comparison of immune cell proportions between cancer and normal tissues in the GSE32424 dataset. C. Immune cell infiltration levels were

compared between high and low LAMP5 expression groups to identify significant differences. D. KEGG pathway enrichment analysis revealed immune-related pathways associated with LAMP5 expression. NK cells activated: Activated natural killer cells; NK cells resting: Resting natural killer cells; TGF-beta signaling pathway: Transforming growth factor-beta signaling pathway; JAK-STAT signaling pathway: Janus kinase-signal transducer and activator of transcription signaling pathway; WNT signaling pathway: Wingless-related integration site signaling pathway; LAMP5: Lysosomal-associated membrane protein 5; KEGG: Kyoto encyclopedia of genes and genomes. *P<0.05, **P<0.01, ***P<0.001, ****P<0.0001, ns: not significant.

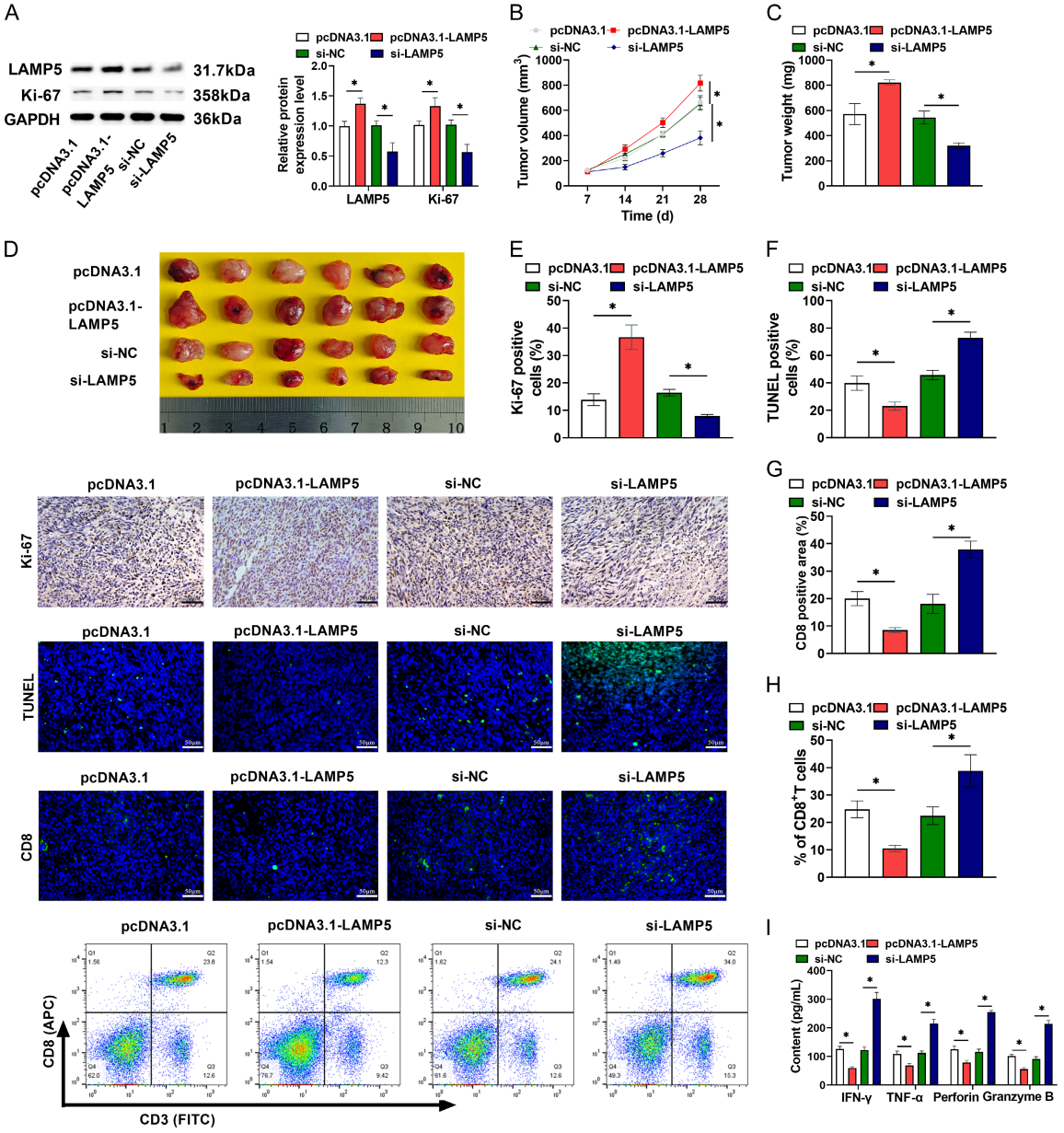

Figure 7. LAMP5 inhibits CD8$^+$ T cell activation and promotes tumor growth *in vivo*. A. Western blot detected LAMP5 and Ki-67 protein levels. B-D. Tumor volumes were recorded weekly. On day 28, tumors were excised, weighed, and photographed. E. IHC assessment of Ki-67 levels (magnification: 40ific). F. Tumor tissue apoptosis was detected by TUNEL staining (magnification: 40ific). G. Immunofluorescence detected CD8 expression (magnification: 40ific). H. The percentage of CD8$^+$ T cells was assessed using flow cytometry. I. ELISA kits were used to detect TNF-he detectiperforin, and granzyme B levels in mouse serum. GAPDH: Glyceraldehyde-3-phosphate dehydrogenase; APC: Allophycocyanin; FITC: Fluorescein isothiocyanate; CD8$^+$ T cells: Cluster of differentiation 8 positive T lymphocytes; Ki-67: Ki-67 protein (named after Kiel, Germany and clone number 67); pcDNA3.1: Plasmid Cytomegalovirus DNA 3.1 (empty vector control); pcDNA3.1-LAMP5: pcDNA3.1 vector expressing lysosomal-associated membrane protein

5; si-NC: Small interfering RNA negative control; si-LAMP5: Small interfering RNA targeting LAMP5; LAMP5: Lysosomal-associated membrane protein 5; ESCC: Esophageal squamous cell carcinoma; TNF-MP5: pcDNA3.1 vector expressing lysosomal-associated membrane protein 5; si-NC: Small interferinynucleotidyl transferase dUTP nick end labeling; ELISA: Enzyme-linked immunosorbent assay. *P<0.05.

against tumors, and NK cell deficiencies and reduced function are linked to an unfavorable prognosis in cancer patients [49, 50]. Our study further observed tumor tissues displayed elevated infiltration of M2 macrophages alongside lower proportions of $CD8^+$ T cells and NK cells relative to normal tissues. These findings are consistent with previous reports on the dysregulated immune cell composition within the TME. In addition, ESCC TME heterogeneity was identified an immunosuppressive phenotype marked by dysfunctional DCs and co-depletion of plasma cells/Tfh cells, correlating with poor prognosis. Resting DC accumulation likely impairs antigen presentation, while plasma cell/Tfh loss disrupts antibody-dependent cytotoxicity and germinal center reactions, creating a "dual-chain immunosuppression" axis [51, 52]. Bioinformatics analysis was conducted to reveal that LAMP5 expression was negatively correlated with Tfh cell infiltration in ESCC. Co-culturing TE1 cells overexpressing LAMP5 with $CD8^+$ T cells reduced the activation rate of $CD8^+$ T cells and weakened their cytotoxic effect on TE1 cells. Furthermore, *in vivo* overexpression of LAMP5 in mice also significantly inhibited $CD8^+$ T cell infiltration. This result aligns with the aforementioned bioinformatics findings. Additionally, LAMP5 expression was correlated with immune-related pathways. These findings might help clarify the relationship between LAMP5 expression and prognostic outcomes in ESCC patients.

However, this study also has certain limitations. This study used subcutaneous injection of mEC25 cells to construct a mouse subcutaneous tumor model. This model cannot fully simulate the in situ microenvironment of human ESCC, which may lead to discrepancies between *in vivo* experimental results and clinical realities. This study only focused on $CD8^+$ T cells, and the regulatory effects of LAMP5 on other immune cells such as macrophages, NK cells, and B cells remain unclear. Additionally, our validation cohort consisted of 65 ESCC patients, which limited our ability to verify the 5-year survival prediction of the prognostic risk signature. Therefore, the sample size could be expanded in the future to further confirm our findings.

In summary, this study identifies a four-gene prognostic signature for ESCC and reveals that LAMP5 promotes ESCC proliferation, invasion and immune escape by inhibiting $CD8^+$ T cell function. These findings provide new prognostic biomarkers and potential immunotherapeutic targets for ESCC, with important translational value for prognosis and treatment.

Conclusion

In conclusion, our analysis of DEGs in ESCC led to the identification of a four-gene prognostic signature. This model has been verified as an independent prognostic factor. Meanwhile, we constructed a nomogram that integrates the gene signatures and clinicopathological features to predict individualized survival probabilities for ESCC patients. LAMP5 overexpression can promote the malignant biological behavior of ESCC cells while inhibiting their apoptosis; more importantly, LAMP5 overexpression can effectively inhibit $CD8^+$ T cell activation. *In vivo* experiments further confirmed that LAMP5 overexpression can inhibit $CD8^+$ T cell activation in a mouse model, thereby promoting tumor growth. This study clarified the key role of LAMP5 in the progression and immune escape of ESCC, providing new theoretical basis and experimental support for the prognostic assessment of ESCC and the development of immunotherapy targets.

Acknowledgements

This study was supported by Hebei Natural Science Foundation (No. H2022206326); Doctor Foundation of Hebei University of Chinese Medicine (No. BSZ2021025); and Medical Science Research Project of Hebei (No. 20221489).

All participants in this study signed informed consent documentation.

Disclosure of conflict of interest

None.

Address correspondence to: Supeng Shen, Biological Tissue Specimen Bank, Hebei Cancer Institute, The Fourth Hospital of Hebei Medical University, No. 12 Jiankang Road, Shijiazhuang 050011, Hebei, China. E-mail: shen48401442@hebmu.edu.cn

References

[1] Zhong L, Li H, Chang W, Ao Y, Wen Z and Chen Y. TP53 mutations in esophageal squamous cell carcinoma. Front Biosci (Landmark Ed) 2023; 28: 219.

[2] Codipilly DC and Wang KK. Squamous cell carcinoma of the esophagus. Gastroenterol Clin North Am 2022; 51: 457-484.

[3] Waters JK and Reznik SI. Update on management of squamous cell esophageal cancer. Curr Oncol Rep 2022; 24: 375-385.

[4] Peng H, He Y, Hu Y, Sheng S, Maitiyasen M, Li J, Liu Y, Hou X, Song H and Yi J. Berbamine promotes ferroptosis of esophageal squamous cell carcinoma by facilitating USP51-mediated GPX4 ubiquitination and degradation. Biomed Pharmacother 2024; 179: 117309.

[5] Qiu S, Hu Y and Dong S. Pan-cancer analysis reveals the expression, genetic alteration and prognosis of pyroptosis key gene GSDMD. Int Immunopharmacol 2021; 101: 108270.

[6] Zhou W, Chen H, Ruan Y, Zeng X and Liu F. High expression of TRIM15 is associated with tumor invasion and predicts poor prognosis in patients with gastric cancer. J Invest Surg 2021; 34: 853-861.

[7] Li G, Feng H, Chen Q, Xue C, Li M, Liu X and Ma S. Identification of immune infiltration-related LncRNA FAM83C-AS1 for predicting prognosis and immunotherapy response in colon cancer. Transpl Immunol 2021; 69: 101481.

[8] Liu X, Liu M, Ma H, Wang J and Zheng Y. miR-875 serves as a candidate biomarker for detection and prognosis and is correlated with PHH3 index levels in breast cancer patients. Clin Breast Cancer 2022; 22: e199-e205.

[9] Zhu K, Xiaoqiang L, Deng W, Wang G and Fu B. Development and validation of a novel lipid metabolism-related gene prognostic signature and candidate drugs for patients with bladder cancer. Lipids Health Dis 2021; 20: 146.

[10] Yousafzai IK, Mehreen A, Noreen N, Ahmad H, Fatima N and Tariq K. Frontiers in cancer and haematology: emerging biomarkers, therapeutics, and technologies. Curr Cancer Res 2025; 1: 54-68.

[11] Guo W, Zhou B, Yang Z, Liu X, Huai Q, Guo L, Xue X, Tan F, Li Y, Xue Q, Gao S and He J. Integrating microarray-based spatial transcriptomics and single-cell RNA-sequencing reveals tissue architecture in esophageal squamous cell carcinoma. EBioMedicine 2022; 84: 104281.

[12] Yu G, Wang LG, Han Y and He QY. clusterProfiler: an R package for comparing biological themes among gene clusters. OMICS 2012; 16: 284-287.

[13] Blanche P, Dartigues JF and Jacqmin-Gadda H. Estimating and comparing time-dependent areas under receiver operating characteristic curves for censored event times with competing risks. Stat Med 2013; 32: 5381-5397.

[14] Zhao R, Zhao D, Zhu X, Li F, Xiong P, Li S and Liu J. The influence of miR-3149 on the malignancy progression of gastric cancer by negatively regulating CEACAM5. J Cancer Biomol Ther 2024; 1: 1-10.

[15] Hu X, Cao D, Zhou Z, Wang Z, Zeng J and Hong WX. Single-cell transcriptomic profiling reveals immune cell heterogeneity in acute myeloid leukaemia peripheral blood mononuclear cells after chemotherapy. Cell Oncol (Dordr) 2024; 47: 97-112.

[16] Cui Y, Li J, Zhang P, Yin D, Wang Z, Dai J, Wang W, Zhang E and Guo R. B4GALT1 promotes immune escape by regulating the expression of PD-L1 at multiple levels in lung adenocarcinoma. J Exp Clin Cancer Res 2023; 42: 146.

[17] Dong LF, Chen FF, Fan YF, Zhang K and Chen HH. Circ-0000512 inhibits PD-L1 ubiquitination through sponging miR-622/CMTM6 axis to promote triple-negative breast cancer and immune escape. J Immunother Cancer 2023; 11: e005461.

[18] Du S, Li P, Liu Y, Cai B, Li G, Wang W, Yan R, Zheng X and Bai T. FOXM1 upregulation, promotes immune escape in gastric cancer through activation of Notch signaling pathway. Mol Cell Biochem 2025; 480: 5411-5427.

[19] Qin X, Li H, Wu J, Tang W, Li W and Li K. PGM5-AS1 promotes progression of diffuse large B-cell lymphoma and immune escape by regulating miR-503-5p. J Inflamm Res 2024; 17: 4187-4197.

[20] Yin Z, Zhang H, Zhang K, Yue J, Tang R, Wang Y, Deng Q and Yu Q. Impacts of combining PD-L1 inhibitor and radiotherapy on the tumour immune microenvironment in a mouse model of esophageal squamous cell carcinoma. BMC Cancer 2025; 25: 474.

[21] Song X, Song Q, Ma X, Xu A and Tian C. MINDY1 induces PD-L1 deubiquitination to promote immune escape in hepatocellular carcinoma by the Wnt/β-catenin pathway. Oncol Res 2025; 33: 3583-3603.

[22] Beeraka NM, Nagalakshmi A, Satyavathi A, Kote DM, Reddy YP, Basappa B, Nikolenko VN, Bannimath G, Bulygin KV and P A M. Ginsenoside Rh4 suppresses Notch3 and PI3K/Akt

pathway to inhibit growth and metastasis of gastric cancer cells. J Cancer Biomol Ther 2025; 2: 145-156.
[23] Yang Q, Cai B, Zhu S, Tai G and Shen A. Identification and validation of MYADM as a novel prognostic marker related to EMT in ESCC. J Cancer 2024; 15: 5351-5366.
[24] Newman AM, Liu CL, Green MR, Gentles AJ, Feng W, Xu Y, Hoang CD, Diehn M and Alizadeh AA. Robust enumeration of cell subsets from tissue expression profiles. Nat Methods 2015; 12: 453-457.
[25] Pastushenko I and Blanpain C. EMT transition states during tumor progression and metastasis. Trends Cell Biol 2019; 29: 212-226.
[26] Mohan V, Das A and Sagi I. Emerging roles of ECM remodeling processes in cancer. Semin Cancer Biol 2020; 62: 192-200.
[27] Baksh SC, Todorova PK, Gur-Cohen S, Hurwitz B, Ge Y, Novak JSS, Tierney MT, Dela Cruz-Racelis J, Fuchs E and Finley LWS. Extracellular serine controls epidermal stem cell fate and tumour initiation. Nat Cell Biol 2020; 22: 779-790.
[28] Janiszewska M, Primi MC and Izard T. Cell adhesion in cancer: beyond the migration of single cells. J Biol Chem 2020; 295: 2495-2505.
[29] Läubli H and Borsig L. Altered cell adhesion and glycosylation promote cancer immune suppression and metastasis. Front Immunol 2019; 10: 2120.
[30] Debnath P, Huirem RS, Dutta P and Palchaudhuri S. Epithelial-mesenchymal transition and its transcription factors. Biosci Rep 2022; 42: BSR20211754.
[31] Ryan AT, Kim M and Lim K. Immune cell migration to cancer. Cells 2024; 13: 844.
[32] Zuo S, Wei M, Zhang H, Chen A, Wu J, Wei J and Dong J. A robust six-gene prognostic signature for prediction of both disease-free and overall survival in non-small cell lung cancer. J Transl Med 2019; 17: 152.
[33] Wu Z, Wang L, Wen Z and Yao J. Integrated analysis identifies oxidative stress genes associated with progression and prognosis in gastric cancer. Sci Rep 2021; 11: 3292.
[34] Liu L, Xiao Y, Wei D, Wang Q, Zhang JK, Yuan L and Bai GQ. Development and validation of a nomogram for predicting suicide risk and prognostic factors in bladder cancer patients following diagnosis: a population-based retrospective study. J Affect Disord 2024; 347: 124-133.
[35] Zhang W, Ji L, Wang X, Zhu S, Luo J, Zhang Y, Tong Y, Feng F, Kang Y and Bi Q. Nomogram predicts risk and prognostic factors for bone metastasis of pancreatic cancer: a population-based analysis. Front Endocrinol (Lausanne) 2022; 12: 752176.
[36] Bai H, Wei X, Yan X, Wei S, Dai S, Wang D, Xue Y, Jana D, Gao F, Zhou W and Zhao L. GRHL3 specifically initiated by the TP63 transcription factor promotes the metastasis of squamous cell carcinogenesis. Cell Signal 2025; 132: 111794.
[37] Fang L, Che Y, Zhang C, Huang J, Lei Y, Lu Z, Sun N and He J. PLAU directs conversion of fibroblasts to inflammatory cancer-associated fibroblasts, promoting esophageal squamous cell carcinoma progression via uPAR/Akt/NF-κB/IL8 pathway. Cell Death Discov 2021; 7: 32.
[38] Yuan S, Bacchetti R, Adams J, Cuffaro D, Rossello A, Nuti E, Santamaria S and Rainero E. The protease ADAMTS5 controls ovarian cancer cell invasion, downstream of Rab25. FEBS J 2025; 292: 4491-4515.
[39] Tong M, Chan KW, Bao JY, Wong KY, Chen JN, Kwan PS, Tang KH, Fu L, Qin YR, Lok S, Guan XY and Ma S. Rab25 is a tumor suppressor gene with antiangiogenic and anti-invasive activities in esophageal squamous cell carcinoma. Cancer Res 2012; 72: 6024-6035.
[40] Ledergor G, Weiner A, Zada M, Wang SY, Cohen YC, Gatt ME, Snir N, Magen H, Koren-Michowitz M, Herzog-Tzarfati K, Keren-Shaul H, Bornstein C, Rotkopf R, Yofe I, David E, Yellapantula V, Kay S, Salai M, Ben Yehuda D, Nagler A, Shvidel L, Orr-Urtreger A, Halpern KB, Itzkovitz S, Landgren O, San-Miguel J, Paiva B, Keats JJ, Papaemmanuil E, Avivi I, Barbash GI, Tanay A and Amit I. Single cell dissection of plasma cell heterogeneity in symptomatic and asymptomatic myeloma. Nat Med 2018; 24: 1867-1876.
[41] Combes A, Camosseto V, N'Guessan P, Argüello RJ, Mussard J, Caux C, Bendriss-Vermare N, Pierre P and Gatti E. BAD-LAMP controls TLR9 trafficking and signalling in human plasmacytoid dendritic cells. Nat Commun 2017; 8: 913.
[42] Umeda S, Kanda M, Shimizu D, Nakamura S, Sawaki K, Inokawa Y, Hattori N, Hayashi M, Tanaka C, Nakayama G and Kodera Y. Lysosomal-associated membrane protein family member 5 promotes the metastatic potential of gastric cancer cells. Gastric Cancer 2022; 25: 558-572.
[43] Lei X, Lei Y, Li JK, Du WX, Li RG, Yang J, Li J, Li F and Tan HB. Immune cells within the tumor microenvironment: biological functions and roles in cancer immunotherapy. Cancer Lett 2020; 470: 126-133.
[44] Han S, Wang W, Wang S, Yang T, Zhang G, Wang D, Ju R, Lu Y, Wang H and Wang L. Tumor microenvironment remodeling and tumor therapy based on M2-like tumor associated macrophage-targeting nano-complexes. Theranostics 2021; 11: 2892-2916.

[45] Marzagalli M, Ebelt ND and Manuel ER. Unraveling the crosstalk between melanoma and immune cells in the tumor microenvironment. Semin Cancer Biol 2019; 59: 236-250.
[46] Zheng Y, Chen Z, Han Y, Han L, Zou X, Zhou B, Hu R, Hao J, Bai S, Xiao H, Li WV, Bueker A, Ma Y, Xie G, Yang J, Chen S, Li H, Cao J and Shen L. Immune suppressive landscape in the human esophageal squamous cell carcinoma microenvironment. Nat Commun 2020; 11: 6268.
[47] Vilbois S, Xu Y and Ho PC. Metabolic interplay: tumor macrophages and regulatory T cells. Trends Cancer 2024; 10: 242-255.
[48] Philip M and Schietinger A. CD8(+) T cell differentiation and dysfunction in cancer. Nat Rev Immunol 2022; 22: 209-223.
[49] Viel S, Vivier E, Walzer T and Marçais A. Targeting metabolic dysfunction of CD8 T cells and natural killer cells in cancer. Nat Rev Drug Discov 2025; 24: 190-208.
[50] Shimasaki N, Jain A and Campana D. NK cells for cancer immunotherapy. Nat Rev Drug Discov 2020; 19: 200-218.
[51] Mandal R, Şenbabaoğlu Y, Desrichard A, Havel JJ, Dalin MG, Riaz N, Lee KW, Ganly I, Hakimi AA, Chan TA and Morris LG. The head and neck cancer immune landscape and its immunotherapeutic implications. JCI Insight 2016; 1: e89829.
[52] Leca J, Lemonnier F, Meydan C, Foox J, El Ghamrasni S, Mboumba DL, Duncan GS, Fortin J, Sakamoto T, Tobin C, Hodgson K, Haight J, Smith LK, Elia AJ, Butler D, Berger T, de Leval L, Mason CE, Melnick A, Gaulard P and Mak TW. IDH2 and TET2 mutations synergize to modulate T Follicular Helper cell functional interaction with the AITL microenvironment. Cancer Cell 2023; 41: 323-339, e310.